Marine Geology 445 (2022) 106758

Contents lists available at ScienceDirect

Marine Geology

journal homepage: www.elsevier.com/locate/margo

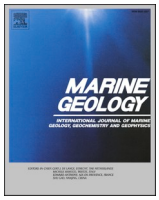

$^{87}Sr/^{86}Sr$ of coral reef carbonate strata as an indicator of global sea level fall: Evidence from a 928.75-m-long core in the South China Sea

Yang Yang [a], Kefu Yu [a,b,*], Rui Wang [a], Tianlai Fan [a], Wei Jiang [a], Shendong Xu [a], Yinqiang Li [a], Jianxin Zhao [c]

[a] Guangxi Laboratory on the Study of Coral Reefs in the South China Sea, Coral Reef Research Center of China, School of Marine Sciences, Guangxi University, Nanning 530004, China
[b] Southern Marine Science and Engineering Guangdong Laboratory (Zhuhai), Zhuhai 519080, China
[c] Radiogenic Isotope Facility, School of Earth and Environmental Sciences, The University of Queensland, Brisbane, QLD 4072, Australia

ARTICLE INFO

Editor: Adina Paytan

Keywords:
Coral reef carbonate strata
Strontium isotopic composition
Global sea level fall
Exposed surface
Late Cenozoic
Northern South China Sea

ABSTRACT

Reconstructing the precise timing of sea level fall is important for understanding earth system during the geologic time. However, previous studies are limited by the absence of effective indicators for sea level fall. To overcome this limitation, we investigated the $^{87}Sr/^{86}Sr$ and petrologic features of carbonate strata in a 928.75-m-long coral reef core (CK2) from Xisha Islands, northern South China Sea and their relationship to sea level fluctuations. Ten exposed surfaces were identified by their petrologic features. The Mn and Sr content, Mn/Sr, Sr/Ca and $\delta^{18}O$ suggest that most of the coral reef carbonate in the CK2 core preserved the original seawater $^{87}Sr/^{86}Sr$ except at intervals of 672–616, 596–575, 521–491, 423–414, and 192.5–161 m, which suffered alteration of meteoric water and showed higher $^{87}Sr/^{86}Sr$ during low sea level period. The 160 carbonate $^{87}Sr/^{86}Sr$ showed a continuously increasing trend, which is consistent with that of seawater over the same period. The continuously increasing $^{87}Sr/^{86}Sr$ curve of CK2 was divided into seven units by six $^{87}Sr/^{86}Sr$ hiatuses. Inconsistency between the sedimentation rate of CK2 and tectonic subsidence rate in the Xisha area suggest that the continuously increasing $^{87}Sr/^{86}Sr$ was controlled by the coupled effect of tectonic subsidence and sea level change, and the hiatus and higher $^{87}Sr/^{86}Sr$ interval in the $^{87}Sr/^{86}Sr$ curve were controlled by sea level fall. The higher $^{87}Sr/^{86}Sr$ usually produced during low sea level (<5 m), $^{87}Sr/^{86}Sr$ hiatus usually produced when sea level changed from deeper to shallower. The depth of hiatuses and higher intervals of $^{87}Sr/^{86}Sr$ correspond well with the exposed surface in CK2 core, verifying that the hiatuses and higher intervals of $^{87}Sr/^{86}Sr$ in the coral reef carbonate succession provide an effective indicator of sea level fall. Using this indicator and the CK2 $^{87}Sr/^{86}Sr$ profile, we identified eleven large-scale sea level falls and three dramatic regressions during 19.6–0.2 Ma and constrained the age based on strontium isotope stratigraphy. These interpreted sea level falls are mostly consistent with other records of global sea level changes, confirming the reliability of our records. The $^{87}Sr/^{86}Sr$ profile of a coral reef carbonate is an efficient indicator of past sea level falls, including their timing.

1. Introduction

Sea level fluctuation was always coupled with global climate change during the Cenozoic (Hodell et al., 1986; Shackleton, 1987; Lambeck and Chappell, 2001; Lambeck and Purcell, 2005; Sano, 2006; Milne et al., 2009; Gasson et al., 2012), as global sea level fluctuation is induced by temperature change on the million-year scale (Miller et al., 2005). For example, the permanent establishment of the East Antarctic Ice Sheet resulted in a sea-level fall of 45–55 m (John et al., 2004), and the sea-level dropped by 121 ± 5 m during the last glacial maximum (Fairbanks, 1989; Peltier and Fairbanks, 2006). The global climate transitioned from a relatively greenhouse-like climate to a cooler climate with a single ice sheet (Miocene), and finally to an icehouse-like climate with polar ice sheets (Quaternary) (Zachos et al., 2001). Therefore, reconstructing the timing and magnitude of sea level fall during the late Cenozoic, particularly since the Miocene, can improve the understanding of global cooling during the Cenozoic.

Atoll carbonate strata are ideal records of sea level fall because the

* Corresponding author at: School of Marine Sciences, Guangxi University, 100# East Daxue Road, Nanning 530004, China.
E-mail address: kefuyu@scsio.ac.cn (K. Yu).

https://doi.org/10.1016/j.margeo.2022.106758
Received 19 June 2021; Received in revised form 13 February 2022; Accepted 14 February 2022
Available online 16 February 2022

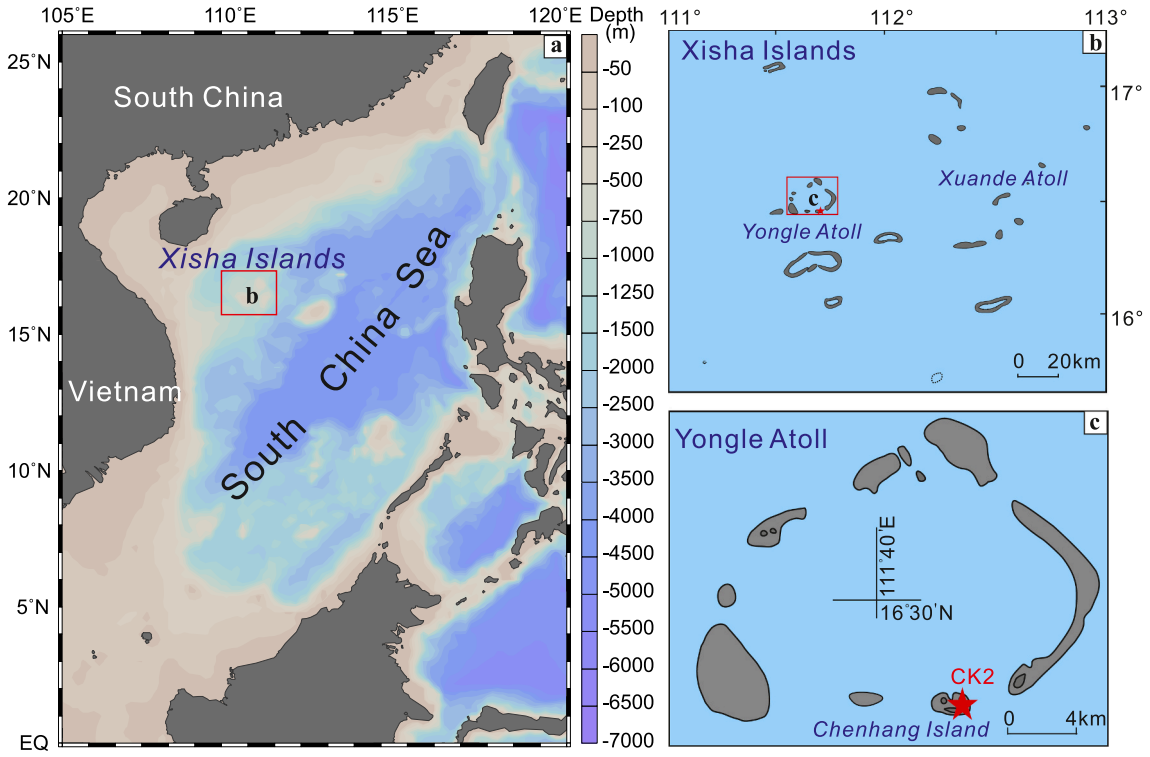

Fig. 1. Geological map of the South China Sea and the sample location of CK2. (a) Map of the South China Sea. (b) Map of Xisha Islands. (c) Map of Yongle Atoll and the location of CK2.

development of coral reefs is sensitive to sea level fluctuation. The depositional history and diagenesis of atolls are controlled by subsidence/uplift and sea-level change. During global sea-level fall or tectonic uplift, an atoll emerges and the shallow carbonate sediment is exposed to erosion and diagenetic alteration (Ludwig et al., 1988; Lincoln and Schlanger, 1991; Ohde and Elderfield, 1992). However, most sea level fall records in coral reefs are concentrated to short time scales (Schlanger and Premoli Silva, 1986; Fairbanks, 1989; Camoin et al., 2001; Sano, 2006) because of a lack of high-resolution dating methods and no clear and uniform indicator. For example, using biostratigraphy, the sea-level fall recorded by turbiditic rocks and stratigraphic hiatus and solution unconformity, which are identified by karst surfaces and fresh-water lens, in Enewetak atoll record the sea level fall at only 25, 31, and 36 Ma (Schlanger and Silva, 1986). Other indicators, such as organisms inhabiting shallow water including *Acropora palmata*, can be used to reconstruct the sea level fall at the last glacial maximum (Fairbanks, 1989). However, widely applying these descriptive indicators on the long-term scale is difficult. Therefore, quantitative indicators must be developed.

The evolution of the coral reef strata $^{87}Sr/^{86}Sr$ ratio has important potential as an indicator of sea level fall. First, sea level fluctuations can determine coral reef development, thereby controlling the evolution of coral reef strata $^{87}Sr/^{86}Sr$. Coral reef carbonate can record contemporary seawater $^{87}Sr/^{86}Sr$ (Edwards et al., 2015), as Sr in coral reefs is derived from seawater during their formation. The development of coral reefs is restricted during low sea level periods, limiting the availability of reef sediments to record the seawater $^{87}Sr/^{86}Sr$ (Ludwig et al., 1988; Lincoln and Schlanger, 1991). In addition, alterations during periods of low sea level can modify $^{87}Sr/^{86}Sr$ (Ohde and Elderfield, 1992; Veizer et al., 1997). Second, previous studies established a highly detailed and accurate seawater $^{87}Sr/^{86}Sr$ evolution curve for the Phanerozoic (Burke et al., 1982; Hess et al., 1986; Hodell and Woodruff, 1994; McArthur et al., 2001, 2016; Prokoph et al., 2008). Particularly, the $^{87}Sr/^{86}Sr$ ratio increased continuously and monotonically during the Cenozoic, enabling the identification of coral reef strata $^{87}Sr/^{86}Sr$ anomalies during this period. Third, the resolution of strontium isotope stratigraphy is superior to other dating methods and does not require a high sample density as it is not restricted by rock facies and latitude (Depaolo and Ingram, 1985), and is, thus, capable providing a more precise age for carbonate samples.

South China Sea is one of the largest marginal seas worldwide (Fig. 1a) and has well-developed coral reefs, including at Xisha Island, Zhongsha Island, and Nansha Island (Yu and Zhao, 2009). In the past 40 years, eight cores have been drilled on a coral reef carbonate platform, providing substantial information on the lithostratigraphy, biostratigraphy, geochemistry, and related climate and environmental changes (Shao et al., 2017a, 2017b; Wang et al., 2018; Xu et al., 2019; Jiang et al., 2019; Li et al., 2021). Records from Xisha Island indicate that the coral reef in the Xisha area began to develop in the Early Miocene, and continues to develop today, forming hundreds of meters to several kilometers of coral reef carbonate strata (Wu et al., 2014; Fan et al., 2020). Coral reef development responded to sea level fall widely and rapidly during the past 20 Ma (Ma et al., 2011; Shao et al., 2017b). The Chenke-2 well (CK2) is a new deep core at Yongle Atoll, Xisha Island, northern South China Sea (Fig. 1b, c), and the high-resolution chronological framework had been established based on strontium isotope stratigraphy and magnetic stratigraphy (Fan et al., 2020). In this study, we focused on the petrologic features and $^{87}Sr/^{86}Sr$ ratio of the CK2 core to 1) identify the exposed surfaces according to their petrological features, 2) obtain the strontium isotopic composition of the coral reef carbonate sequence in Xisha Island, 3) explore the factors controlling the $^{87}Sr/^{86}Sr$ ratio of the CK2 core, and examine the relationship between shallow carbonate strata $^{87}Sr/^{86}Sr$ and sea level fall, and 4) reconstruct the exact timing of sea level fall since the Miocene, with comparisons to other records to test the reliability of our results.

2. Regional setting

The South China Sea is located in the Tropical Western Pacific Warm Pool. The high precipitation (1300–2000 mm), temperature (22–30 °C),

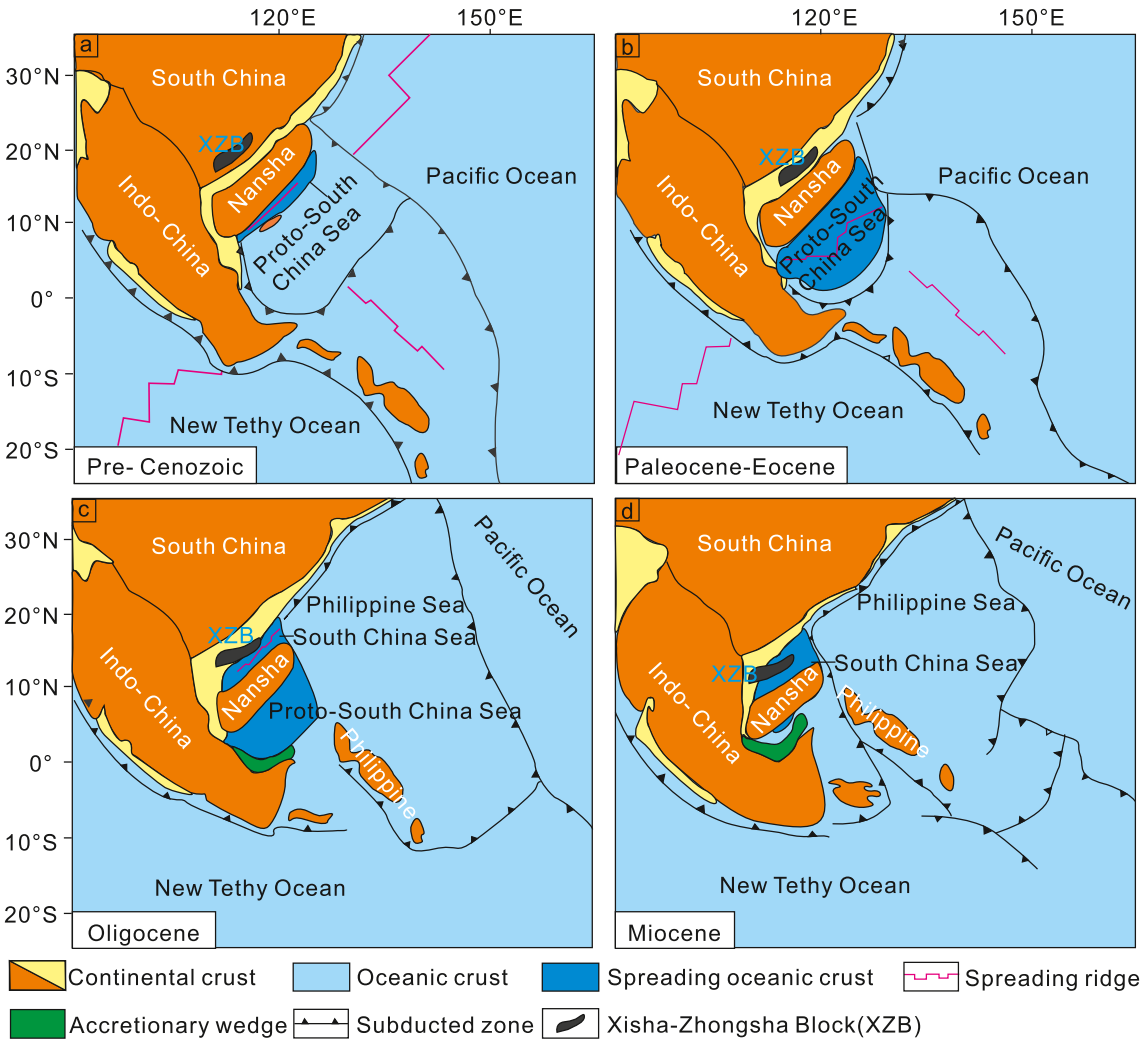

Fig. 2. Schematic diagrams of the tectonic evolution during pre-Cenozoic, Paleocene-Eocene, Oligocene and Miocene. (Revised from Hall, 2012 and Zahirovic et al., 2014).

and salinity (33.14–34.24‰) make it an ideal area for coral reef development (Shao et al., 2017a). Xisha Islands are one of the most well-known carbonate islands in the South China Sea and comprises Yongle Atoll, Xuande Atoll and other coral reefs (Fig. 1b).

Xisha Islands is located in the northwest continental slope of the South China Sea, and its basement is the Xisha-Zhongsha block (Fig. 2a). It separated from the South China continent during the subduction of the paleo-South China Sea in the Eocene-Paleocene (Fig. 2b) and gradually moved away from the South China continent, before moving further southeast with the expansion of the new South China Sea during the Oligocene (Fig. 2c). The northwest sub-basin stopped expanding at the ridge until the late Oligocene, resulting in an end to the lateral growth of the fault depression in the north of the Xisha-Zhongsha block, as well as an end to the migration of the Xisha-Zhongsha block (Fig. 2d). The Xisha-Zhongsha block was still subaerially exposed at the end of the Late Oligocene (Hall, 2012; Fyhn et al., 2009, 2013; Menier et al., 2014; Zahirovic et al., 2014). With thermal subsidence after lithospheric cracking, the Xisha-Zhongsha block gradually sank, and almost all of it becoming submerged in the early Miocene (Fig. 3a). The Xisha Block was surrounded by negative terrain, making it difficult for the river to flow from the adjacent continent at this time. Therefore, the seawater in the Xisha Sea area has remained relatively clean since the Miocene, and the volcanic activities during the Oligocene provide a high geographical position for coral reef initiation (Ma et al., 2011; Zhang et al., 2019). The subsidence rate of the Xisha Block increased gradually, reaching its highest at 10–8.2 Ma, and nearly ceasing during 5–2.6 Ma (Wu et al., 2014). With the subsidence of the Xisha-Zhongsha block and global sea level fluctuation, the coral reef carbonate deposition was initiated in Xisha Island in the Early Miocene (Ma et al., 2011; Shao et al., 2017a; Shao et al., 2017b; Wu et al., 2014; Fan et al., 2020), flourishing and expanding laterally to reach its maximum during the Middle Miocene (Ma et al., 2011) (Fig. 3b), recessing during the Late Miocene (Ma et al., 2011;Wu et al., 2014) (Fig. 3c), and shrinking to an isolated carbonate platform (e.g. Yongle Atoll, Xuande Atoll) (Fig. 1b) during the Pliocene and Pleistocene (Wu et al., 2014) (Fig. 3d).

CK2 is a deep drilling well in a low-lying area near the gravel dam of Chenhang Island, southeast of the Yongle Atoll (Fig. 1c). CK2 is composed of 873.55 m of reef carbonate and 55.2 m of the Oligocene volcanic basement (35.5 ± 0.9 Ma) (Zhang et al., 2019). The average recovery of CK2 was 70%, and the recovery of most coral reef sequences were more than 80%, with well-preserved carbonate. The upper 21.4 m of CK2 is composed of unconsolidated modern deposition, whereas the area below 21.4 m contains different types of limestone and dolomite. The detailed lithologic and biological information have been documented in supplementary material 1. The chronological framework of CK2 was established based on previously published strontium isotope and magnetic stratigraphy (Fan et al., 2020). A total of 60 $^{87}Sr/^{86}Sr$ samples from CK2 were selected for translation into a numerical age (Fig. 4B). The result showed that the coral reef development began at 19.6 Ma, and were drowned until 16.26 Ma, the environment were

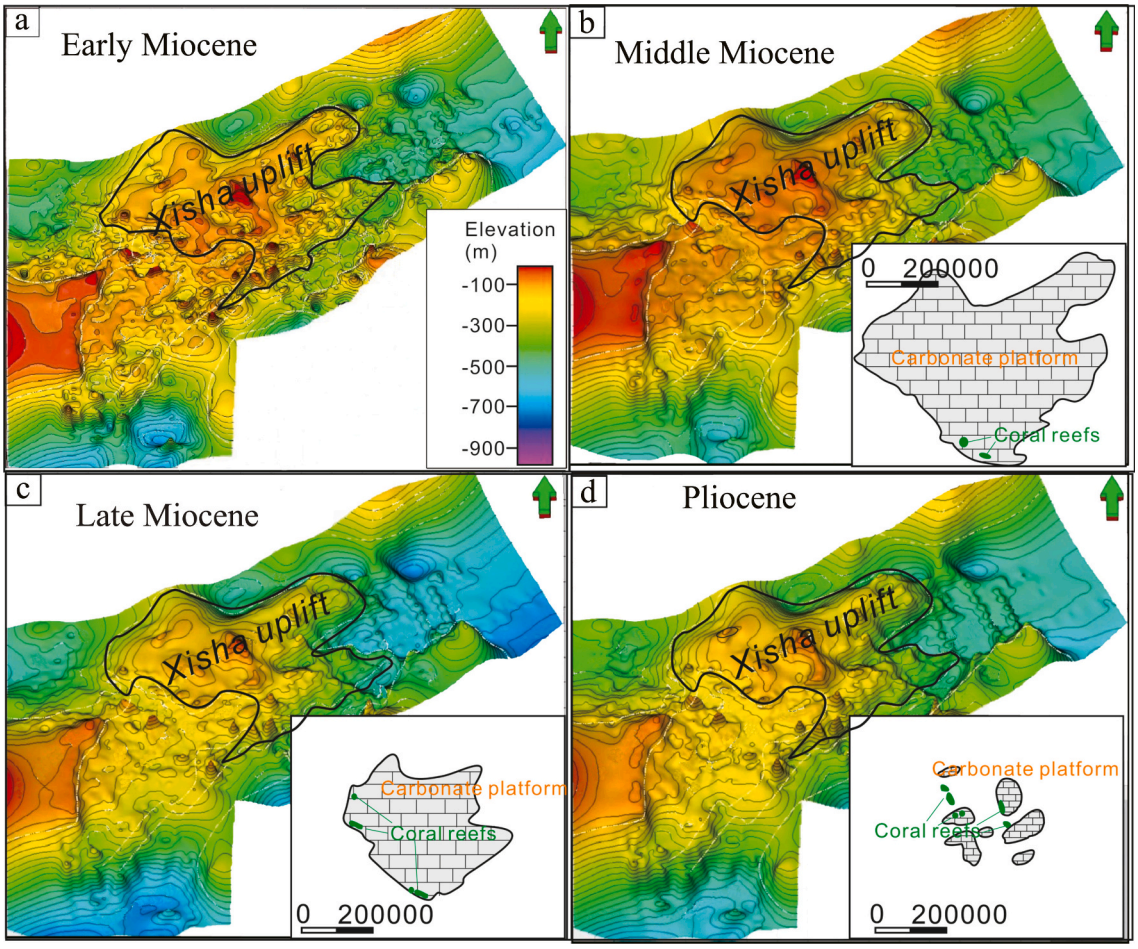

Fig. 3. Schematic diagrams of the paleogeography evolution during Early Miocene, Middle Miocene, Late Miocene and Pliocene. (Revised from Yang, 2014).

lagoon to lagoon slope during 16.26–10.66 Ma, and progressively transformed into a reef crest environment from 10.66–4.36 Ma to 4.36–1.59 Ma, the reef started to be drowned again from 4.36 to present.

3. Materials and methods

3.1. Sample selection and preparation

Previous Sr isotope data have been published by Fan et al. (2020), aiming to establish a chronological framework for coral reef carbonate formation in Well Chenke 2 (CK2). Their work focused on how to choose suitable samples that preserved the original seawater $^{87}Sr/^{86}Sr$. A total of 100 samples were collected uniformly at fixed intervals (5 m or 10 m) throughout the sequence, and 60 samples were finally selected to match the referenced seawater $^{87}Sr/^{86}Sr$ evolution curve (McArthur et al., 2001) for dating. However, no analysis has been performed on the abnormal $^{87}Sr/^{86}Sr$ and the overall trend of $^{87}Sr/^{86}Sr$ evolution curve of CK2, which may record the change of paleo-climate and paleo-environment. The purpose of the current study is to reconstruct the abnormal paleoclimatic and paleoenvironmental events based on the abnormal $^{87}Sr/^{86}Sr$ and overall trend of the $^{87}Sr/^{86}Sr$ evolution curve of CK2. Therefore, we preferentially selected samples to focus on these anomalies in this study. These abnormal samples were selected in two aspects that are explained as follows:

First, we added 34 samples at intervals of the abnormal $^{87}Sr/^{86}Sr$ based on the $^{87}Sr/^{86}Sr$ curve of CK2 reported by Fan et al. (2020), with the purpose of supplementing the dataset and quantifying the specific strontium isotope offset.

Second, we selected 26 samples at the exposed surface indicated by the lithologic feature, in order to analyze the relationship between the exposed surface and strontium isotopes. The exposed surface was produced by carbonate weathering and eluviation during tectonic uplift or during sea-level fall, characterized by reddish-brown and yellowish-brown materials and calcareous concretion, with karst caves and grikes. These petrologic features were examined by visual and microscopic observation in the 873.55 m core samples and 300 thin sections.

In order to avoid contamination, all of the sixty samples were placed in a glass beaker and cleaned ultrasonically with deionized water for 30 min. The supernatant was removed after 24 h. After triplicate cleaning, the precipitate was dried and ground to less than 200 powder grains in an agate bowl.

3.2. Sr isotopic measurement

For Sr isotopic analysis, approximately 0.1 g of pretreated samples was digested in a mixed solution of HNO_3 (1 mL) + HF (1 mL) in tightly closed Teflon vials at 120 °C for 36 h. After drying, the remaining materials were re-dissolved in 2 N HNO_3 and centrifuged to remove impurities. After removing the supernatant, the sample was purified through specific ion exchange resin. The Sr isotopic composition was measured on a Nu Plasma high-resolution MC-ICP-MS at the Radiogenic Isotope Facility, University of Queensland, Australia. The quality discrimination effect in instrumental analysis was externally corrected by an exponential function. The $^{87}Sr/^{86}Sr$ ratio was normalized to $^{86}Sr/^{88}Sr = 0.1194$. Proton mass deviation was corrected by SRM987, i.e., $^{87}Sr/^{86}Sr = 0.710249 \pm 9$, for every four samples. Ten percent of the samples were tested repeatedly to ensure the quality of the data.

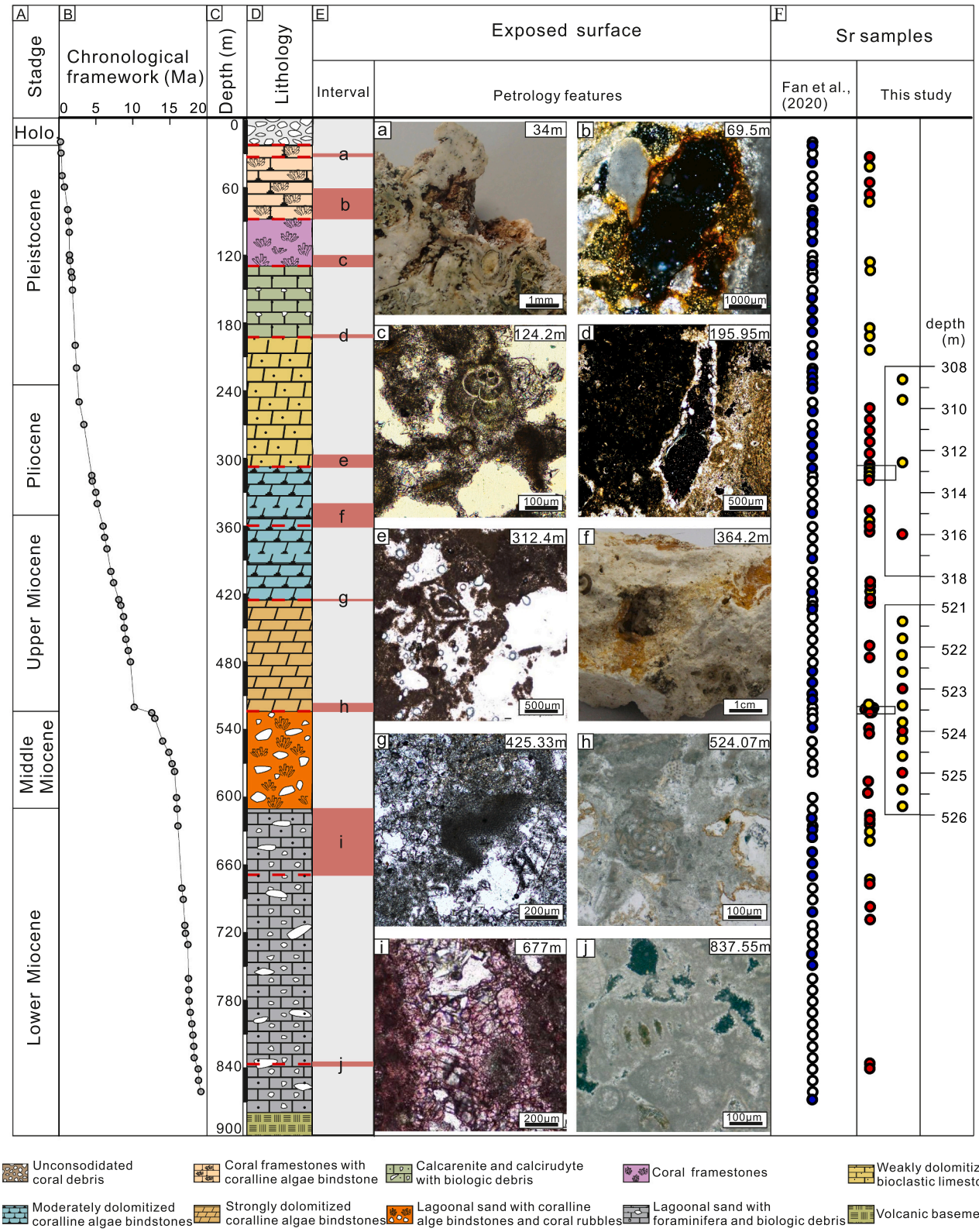

Fig. 4. (A) Stages, (B) chronological framework based on $^{87}Sr/^{86}Sr$ (Fan et al., 2020), (C) depths, (D) lithology, (E) exposed surface interval and petrologic features (a) Reddish-brown and yellowish-brown iron oxides, white calcareous concretion with karst cave and grike on limestone surface. b) Reddish-brown iron oxides under crossed-polarized light. c) Overhanging calcite in foraminiferal micrite limestone vugular pores under plane-polarized light. d) Dissolution pores with sparry rim under crossed-polarized light. e) Dissolution molds of foraminifera. f) Yellowish-brown paleo-weathering crust and dissolution pores on limestone surface. g) Sparry cement and dolomite crystal under crossed-polarized light. h) Yellowish-brown iron oxide at the dissolution mold rim under plane-polarized light. i) Dissolution and recrystallization of biological skeleton under crossed-polarized light. j) Dissolution molds and vugular pores under plan-polarized light.) and (F) specific depths of the selected samples for $^{87}Sr/^{86}Sr$ measurement (white and blue cycles represent samples from Fan et al. (2020); white were used for dating, blue were alteration samples; red circles and yellow represent samples in this study, the yellow were selected at exposed intervals). (For interpretation of the references to colour in this figure legend, the reader is referred to the web version of this article.)

Table 1
The age, Mn and Sr contents, Mn/Sr, Sr/Ca, δ^{18} O, and $^{87}Sr/^{86}Sr$ of CK2.

Depth (m)	Age (Ma)	Mn	Sr	Mn/Sr	Sr/Ca	$\delta^{18}O$		$^{87}Sr/^{88}Sr$	2δ [a] 10^{-6}
33	0.30	52	1275	0.04	3.30			0.709174	9
56	0.58	150	1030	0.15	2.57	−7.81		0.709160	9
66	0.85	59	1044	0.06	2.87	−7.79		0.709159	9
256	2.89	17	311	0.06	0.85	0.92		0.709058	9
266	3.22	35	271	0.13	0.82	1.17		0.709049	8
276	3.50	18	307	0.06	0.84	0.87		0.709037	10
286								0.709036	10
								0.709066	8
	3.74	24	312	0.08	0.80	0.95	Mean	0.709051	9
296	3.97	47	214	0.22	0.58	1.51		0.709050	10
306	4.21	47	258	0.18	0.70	1.47		0.709060	10
316	4.45	24	121	0.20	0.49			0.709033	9
346	5.38	27	201	0.14	0.89	4.11		0.709040	9
356	5.78	98	236	0.41	1.06	3.58		0.708970	10
364	6.04	143	227	0.63	0.98	3.47		0.708972	9
414	7.53	19	200	0.09	0.86			0.708979	8
417	7.67	33	293	0.11	1.28			0.708954	8
422	7.91	24	236	0.10	1.01			0.708964	9
423	7.96	32	265	0.12	1.15			0.708970	9
466	9.21	73	417	0.18	0.97			0.708904	9
476	9.53	234	320	0.73	1.40	4.46		0.708927	10
523	11.13	16	331	0.05	0.87	−4.41		0.708811	10
524	11.61	13	285	0.05	0.78			0.708823	9
525	12.08	13	233	0.06	0.61	−3.07		0.708839	11
539								0.708810	8
								0.708810	9
	13.40	20	256	0.08	0.69		Mean	0.708810	8
542	13.56	23	537	0.04	1.44			0.708799	8
586	15.56	56	864	0.06	2.33			0.708798	8
596	15.77	10	281	0.04	1.51			0.708792	10
616								0.708759	8
						−7.14		0.708766	9
	16.08	13	446	0.03	1.15		Mean	0.708762	8
620	16.17	9	310	0.03	0.77			0.708749	10
624	16.21	13	317	0.04	0.81	−2.97		0.708759	8
676	16.59	11	246	0.04	0.63	−7.25		0.708685	9
696	16.87	20	922	0.02	2.38			0.708673	10
707	16.97	38	491	0.08	1.32			0.708666	9
836	18.56	34	271	0.13	1.40			0.708522	9
838	18.67	26	267	0.10	0.69			0.708544	9

[a] The age are based on chronological framework of Fan et al. (2020).

3.3. Oxygen isotope and element measurement

The Mn, Sr, and Ca contents and $\delta^{18}O$ measurement were determined at the Coral Reef Research Center of China, Guangxi University. Carbonate samples for Mn, Sr, and Ca content analyses were measured using a Thermo Fisher Scientific inductively coupled plasma-mass spectrometer. Analyzed data were assessed for accuracy and precision using the quality assurance and quality control (QA/QC) program, which included reagent blanks, duplicate test, and certified geochemical reference materials (GBW07129, GBW07133, GBW07135) with deviation <5%. $\delta^{18}O$ was measured on a Finnigan MAT-253 stable isotope mass spectrometer that attached to a Fairbanks carbonate preparation device. Isotopic ratios were reported in the conventional per mil (‰) notation and normalized to the Vienna Pee Dee Belemnite using the GBW04405 standard ($\delta^{18}O = -8.49‰$).

4. Results

4.1. Petrologic features and sedimentary facies

The detailed petrologic features and sedimentary facies have been documented in supplementary material 1. Most reef carbonate was white or yellowish-white, including coral fragments, foraminifera fossils, and other biologic debris. However, biological fragments at 671–611 m were composed of well-rounded gravel, which obviously differed from the adjacent carbonate strata. The exposed surfaces were observed at 32–34 (a), 60–90 (b), 121–133 (c), 190–196 (d), 294–312.5 (e), 341–361 (f), 426 (g), 518–526 (h) and 611–671 m (i) (Fig. 4E). The rock was characterized by reddish-brown and yellowish-brown iron oxides (Fig. 4Ea, b, f, h), white calcareous concretion (Fig. 4Ea), karst cave, and grike (Fig. 4Ea, f), the selective or non-selective dissolution and mold pores (Fig. 4Ed, g, e, i), new crystals in dissolved pores (Fig. 4Ec, g, j) or sparry cement (Fig. 4Eg).

At a depth of 0–16.29 m, lime-sand islets predominate, whereas 16.29–89.43 m is dominated by an outer reef flat deposit, 89.43–131.13 m by an inner reef flat deposit, 131.13–310.9 m by lagoon slope deposits, 310.29–435 m by outer flat deposits, 435–522 m by inner flat deposits, 522–611 m by lagoon slope deposition, and 611–873.5 m is dominated by a restricted lagoon deposition (Fig. 8d).

4.2. $^{87}Sr/^{86}Sr$ ratios

Considering that the $^{87}Sr/^{86}Sr$ ratios reported here agree with the results of Fan et al. (2020), We characterized the $^{87}Sr/^{86}Sr$ of the CK2 core based on our 60 samples and the 100 samples reported by Fan et al. (2020). As shown in Tables 1 and 2, and Fig. 7A, $^{87}Sr/^{86}Sr$ in the 160 coral reef carbonate strata generally increased with decreasing depth, ranging from 0.708506 at 861 m to 0.709168 at 21 m. The carbonate strata $^{87}Sr/^{86}Sr$ ratios showed three main trends:

(1) Hiatus in the $^{87}Sr/^{86}Sr$ curve, with $^{87}Sr/^{86}Sr$ changed sharply. The hiatus appeared at 836–831, 731–721, 521.4–521, 354.5–351, 316–311, and 71–66 m.

Table 2
The age and $^{87}Sr/^{86}Sr$ of exposed surface from CK2.

Exposed surface		Depth (m)	Age (Ma)		$^{87}Sr/^{88}Sr$	2δ [a] 10^{-6}
a	32–34 m	34.17	0.31		0.709172	8
b	60–90 m	72.50	0.99		0.709151	8
c	121–133	123.50	1.45		0.709099	10
		132.50	1.60		0.709089	10
d	190–196 m	185	2.09		0.709081	8
		192.50	2.15		0.709099	10
		204.50	2.24		0.709086	9
e	294–312.5 m	308.5			0.709079	9
					0.709075	9
			4.27	Mean	0.709077	9
		309.50	4.30		0.709056	8
		312.50	4.37		0.709030	9
f	341–361 m	354.50	5.72		0.708994	8
g	426 m	418.90	7.77		0.708973	9
h	518–526 m	518.50	10.16		0.708838	9
		521.4			0.708822	8
					0.708831	9
			10.38	Mean	0.708826	9
		521.8	10.57		0.708819	10
		522.2			0.708806	8
					0.708796	8
			10.76	Mean	0.708801	8
		522.6	10.95		0.708800	10
		523.4	11.32		0.708822	8
		523.8	11.51		0.708813	10
		524.2	11.70		0.708810	10
		524.6	11.89		0.708909	7
		525.4	12.27		0.708819	9
		525.8	12.46		0.708814	9
i	611–671 m	630.34	16.26		0.708795	11
		637.92	16.31		0.708749	9
		674.07	16.57		0.708709	10

[a] The age are based on chronological framework of Fan et al. (2020).

(2) Carbonate strata $^{87}Sr/^{86}Sr$ continuously increased. These parts were divided into seven units by the Hiatus: 1 (873.5–836 m), 2 (831–731 m), 3 (721–521.4 m), 4 (521–361 m), 5 (341–316 m), 6 (311–71 m), and 7 (61–21 m).
(3) (3) Higher $^{87}Sr/^{86}Sr$ intervals compared with the adjacent interval, appeared at interval I (672–616 m), II (601–578 m), III (521–481 m), IV (426–411 m), and V (201–152 m).

4.3. $\delta^{18}O$ value and Mn, Sr, and Ca contents

As shown in Table 1 and Figs. 5, and 6, the $\delta^{18}O$ value ranged from 4.46 to −7.81, and the correlation coefficient between the $^{87}Sr/^{86}Sr$ and $\delta^{18}O$ values was 0.086. The Sr content ranged from 201 to 1275 ppm, with the exception of 121 ppm recorded at 316 m. The Mn content ranged from 9 to 150 ppm, except for 234 at 476 m. The Mn/Sr ranged from 0.04 to 0.73. The Ca content varied from 107 to 400 ppm, and the Sr/Ca varied between 0.13 and 21.67.

4.4. Assessment of $^{87}Sr/^{86}Sr$ reliability

Shallow bulk carbonate is an ideal recorder of seawater $^{87}Sr/^{86}Sr$ (Edwards et al., 2015). However, carbonate $^{87}Sr/^{86}Sr$ is vulnerable to various alterations during diagenesis and post-depositional processes (Marenco et al., 2008; Jiang et al., 2011; Saltzman and Sedlacek, 2013). External fluid, such as pore water, meteoric water, dolomite fluid, and hydrothermal fluid, react with carbonate to alter the $^{87}Sr/^{86}Sr$ (Brand and Veizer, 1980; Vahrenkamp et al., 1988; Kaufman et al., 1993; Ren and Jones, 2017), thus, it is necessary to assess the degree of these alterations. Previous studies showed that carbonate altered by these external fluids may decrease the Sr content and increase the Mn content, leading to a lower Sr/Ca ratio and higher $\delta^{18}O$. Thus, the shallow bulk carbonate preserves the original seawater $^{87}Sr/^{86}Sr$ with the following limitations: 1) Mn content <250 ppm, 2) Sr content >200 ppm, 3) Mn/Sr

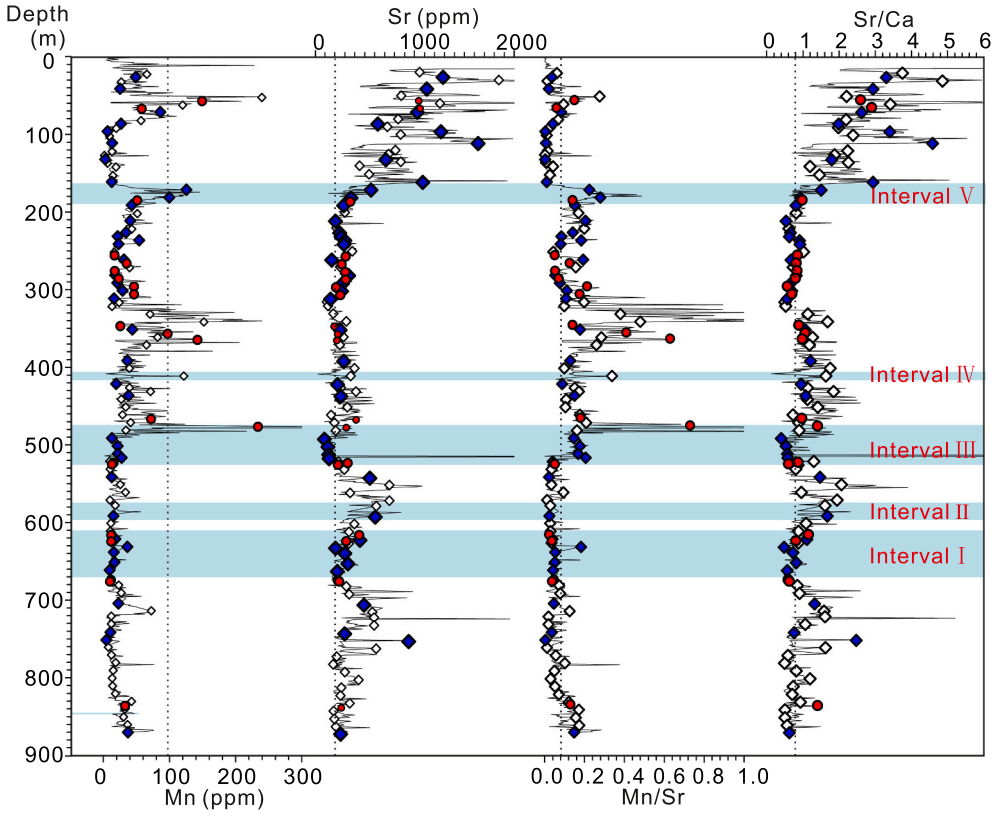

Fig. 5. Evolution curve of the Mn and Sr contents, Mn/Sr ratios, and Sr/Ca ratios with depths in CK2 (red circles are samples in this study, others are from Fan et al. (2020)). (For interpretation of the references to colour in this figure legend, the reader is referred to the web version of this article.)

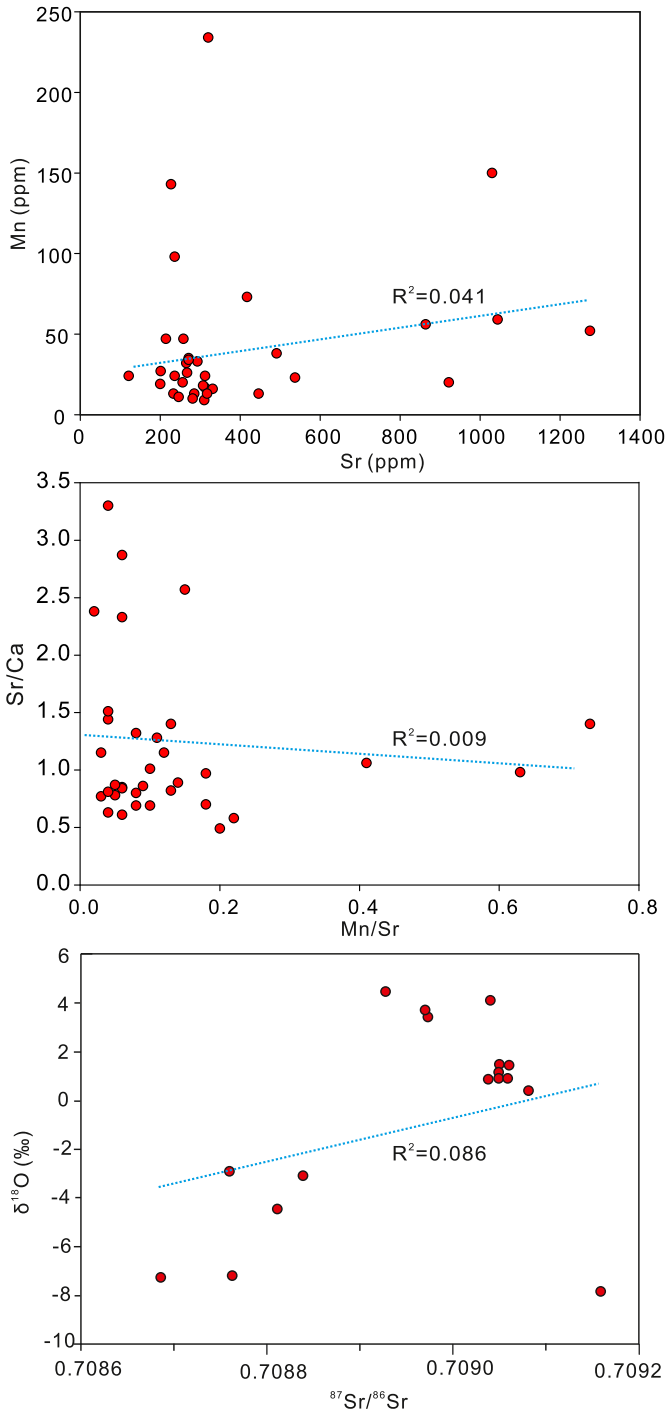

Fig. 6. Correlation of Mn and Sr contents, Mn/Sr and Sr/Ca, $^{87}Sr/^{86}Sr$ and $\delta^{18}O$ of the samples in this study.

<2, and 4) $\delta^{18}O > -10‰$, showing no correlation with $^{87}Sr/^{86}Sr$ (Korte et al., 2003; Derry et al., 1989; Kaufman et al., 1992; Li et al., 2011a). The Mn and Sr contents, Mn/Sr ratio, Sr/Ca ratio, and $\delta^{18}O$ data of the CK2 core are shown in Figs. 5, and 6, revealing that the Mn content in all samples were less than 250 ppm, Mn/Sr ratios were less than 2, except for at 477 m where the Mn content was 620 ppm and Mn/Sr was 2.2, Sr content was typically higher than 200 ppm, the $\delta^{18}O$ value ranged from 4.46 to −7.81, and $^{87}Sr/^{86}Sr$ and $\delta^{18}O$ values showed no correlation. The values described above were used as limits to indicate the degree of altercation. Most element indicators were below the limit, indicating that the coral reef carbonate of the CK2 core was not strongly altered and is within the acceptable range for preservation of the original seawater $^{87}Sr/^{86}Sr$. However, intervals I (672–616 m), II (596–575 m), III (521–491 m), IV (423–414 m), and V (192.5–161 m) were characterized by the lowest Sr/Ca and Sr contents, indicating relatively strong alterations by meteoric water, although most values were under the limits. Particularly, the well-rounded gravel observed in interval I indicated that the carbonate rock at 671–611 m likely formed by erosion and transportation, causing obvious changes in $^{87}Sr/^{86}Sr$. Cathodoluminescence imaging further revealed that the carbonate in interval III was greatly altered (Wang et al., 2018).

4.5. Sr-age of CK2

Strontium isotope stratigraphy is a high-resolution dating method for shallow water carbonates that has been applied to the carbonate strata of multiple coral reefs, such as Enewetak Atoll (Ludwig et al., 1988), Kita-Daito-jima Atoll (Ohde and Elderfield, 1992), and the Hawaiian Islands (Webster et al., 2010). A chronological framework of the CK2 based on strontium isotope stratigraphy and magnetostratigraphy was established by Fan et al. (2020). In their work, 60 samples of the $^{87}Sr/^{86}Sr$ data were selected for conversion to a numerical age using a calibrated standard seawater $^{87}Sr/^{86}Sr$ lookup table (McArthur et al., 2001), other ages were calculated by interpolation as shown in Fig. 4B. Samples collected from the consistently increasing $^{87}Sr/^{86}Sr$ units in this study showed that their $^{87}Sr/^{86}Sr$ were similar to those of Fan et al. (2020), demonstrating that the chronological framework of the increasing $^{87}Sr/^{86}Sr$ units in Fan et al. (2020) is a reliable chronological framework and suitable for dating. However, the chronological framework in Fan et al. (2020) did not consider discontinuity, such as in areas without carbonate deposition, thus, limiting the dating accuracy. We densified the samples at the interval of the $^{87}Sr/^{86}Sr$ hiatus, which showed that the $^{87}Sr/^{86}Sr$ of these samples was uneven and closer to the boundary of consistently increasing $^{87}Sr/^{86}Sr$ units. For example, for Hiatus 3 between Uunit 3 and 4, the $^{87}Sr/^{86}Sr$ of the top of Unit 3 (526 m) was 0.708826, which was converted to a numerical age of 12.55 Ma, and the $^{87}Sr/^{86}Sr$ of the bottom of Unit 4 (521 m) was 0.708884, which was converted to a numerical age of 10.19 Ma. The ten densified samples at an interval of 0.4 m between 526 and 521 m showed that the $^{87}Sr/^{86}Sr$ of all ten samples was closer to that at 526 m (0.708531), suggesting that there is no $^{87}Sr/^{86}Sr$ record for 12.55–10.19 Ma. Therefore, the dating data at the interval of the $^{87}Sr/^{86}Sr$ hiatus cannot be calculated by interpolation. Instead, densifying the samples helped confirm the accurate location of discontinuity, which appeared at 836–831, 731–721, 521.4–521, 354.5–351, 316–311, and 71–66 m. The Sr-age during these intervals should not be considered, as there was no carbonate deposition during these periods.

5. Discussion

5.1. Factors controlling coral reef carbonate $^{87}Sr/^{86}Sr$

Shallow water carbonates can record the original seawater $^{87}Sr/^{86}Sr$ ratio. Globally seawater $^{87}Sr/^{86}Sr$ was homogeneous at the same geologic time, as the $^{87}Sr/^{86}Sr$ residual time in seawater is 2.5 Ma, which is significantly longer than the global seawater mixing time of 1600 years (Peterman et al., 1970; Hodell et al., 1990). Thus, in theory, the $^{87}Sr/^{86}Sr$ of reef carbonates should be consistent with that of seawater. The coral reef carbonate $^{87}Sr/^{86}Sr$ ratios of CK2 increased constantly from the bottom to top, ranging from 0.708509 to 0.709174. This trend, and the range of the $^{87}Sr/^{86}Sr$ ratios, have been consistent with the seawater $^{87}Sr/^{86}Sr$ since 20 Ma (Fig. 7A), indicating that the reef carbonate of the CK2 is primarily related to the global seawater $^{87}Sr/^{86}Sr$. However, the coral reef carbonate $^{87}Sr/^{86}Sr$ of CK2 do not precisely correspond to the seawater $^{87}Sr/^{86}Sr$. For example, the hiatus periods at 836–831, 731–721, 521.4–521, 354.5–351, 316–311, and 71–66 m, as well as the higher $^{87}Sr/^{86}Sr$ at 672–616 m (Interval I), 521–491 m

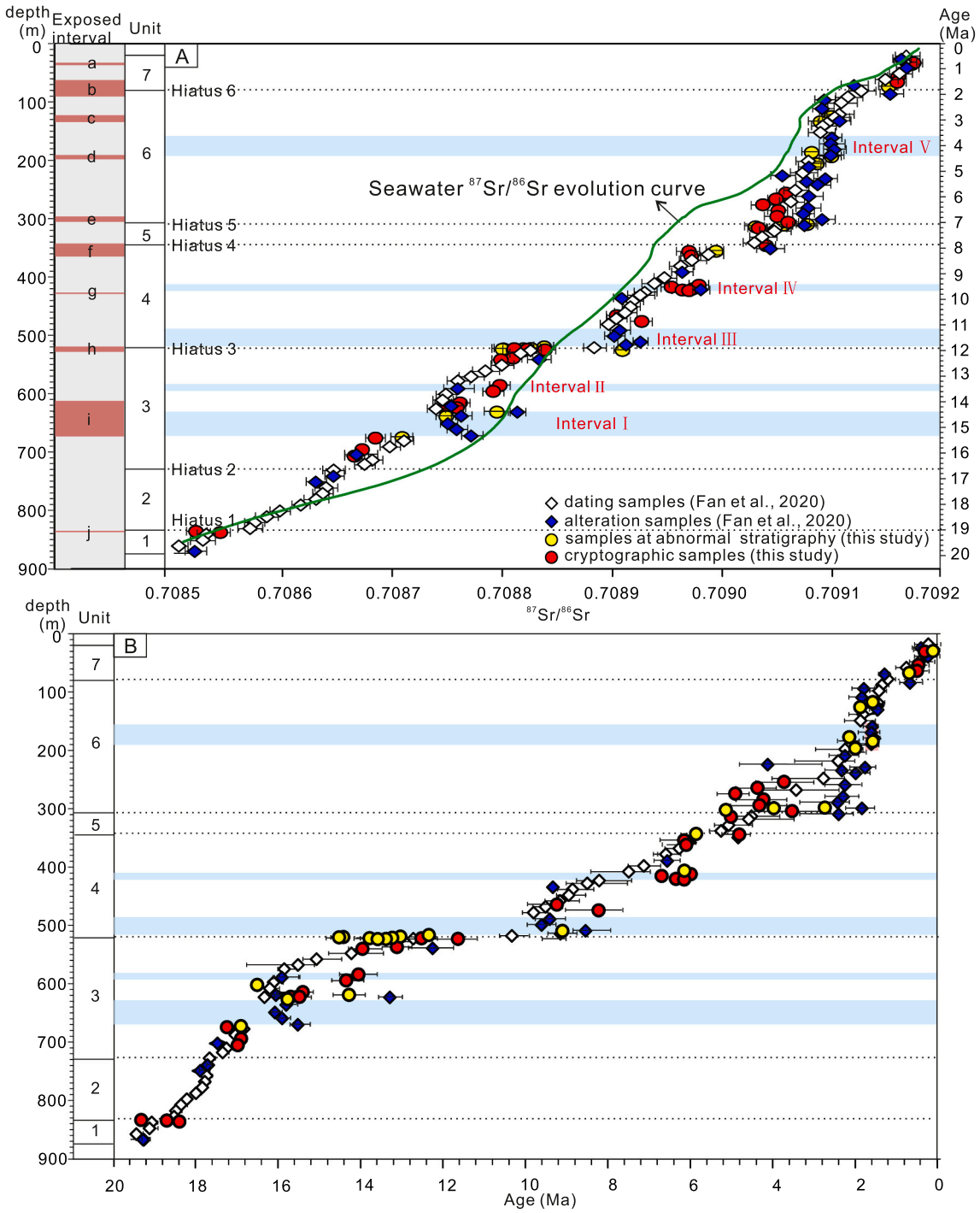

Fig. 7. (A) $^{87}Sr/^{86}Sr$ of coral reef carbonate strata with depth of CK2 and Seawater $^{87}Sr/^{86}Sr$ evolution curve since 20 Ma; (B) the corresponding dating data of $^{87}Sr/^{86}Sr$ with depth based on strontium isotope stratigraphy.

(Interval III), 423–414 m (Interval IV), and 192.5–161 m (Interval V) (Fig. 7A) suggest that other factors, such as the terrigenous material, regional tectonic activities, and sea level change, influence the $^{87}Sr/^{86}Sr$ of CK2.

5.1.1. *Terrigenous material influence*

Seawater $^{87}Sr/^{86}Sr$ is controlled by terrigenous material inputs with a high $^{87}Sr/^{86}Sr$ and hydrothermal material inputs with a low $^{87}Sr/^{86}Sr$ (Depaolo and Ingram, 1985; Palmer and Edmond, 1989; Derry et al., 1989). As a marginal basin, sea-floor spreading, uplift of Tibetan Plateau-Himalayas, Asian monsoon and drought of interior Asian represent the four potential factors impacting the $^{87}Sr/^{86}Sr$ in South China Sea. Therefore, we discuss the influence of regional tectonic activities and climate change on the seawater $^{87}Sr/^{86}Sr$ changes in South China Sea by comparing these four factors and $^{87}Sr/^{86}Sr$ evolution of CK2 in temporal. Obvious regional tectonic activities and climate change occurred at 15 Ma. Sea-floor spreading in the South China Sea basically ceased after 15 Ma (Taylor and Hayes, 1980; Huang et al., 2013; Yan et al., 2015), resulting in decreased input of material with lower $^{87}Sr/^{86}Sr$. While, the uplift of Tibet (Li et al., 2011b), and aridity in the interior Asian (Guo et al., 2002) began after 15 Ma, the strength of the monsoon enhanced after 8 Ma (An et al., 2001; Liu et al., 2007, 2016;

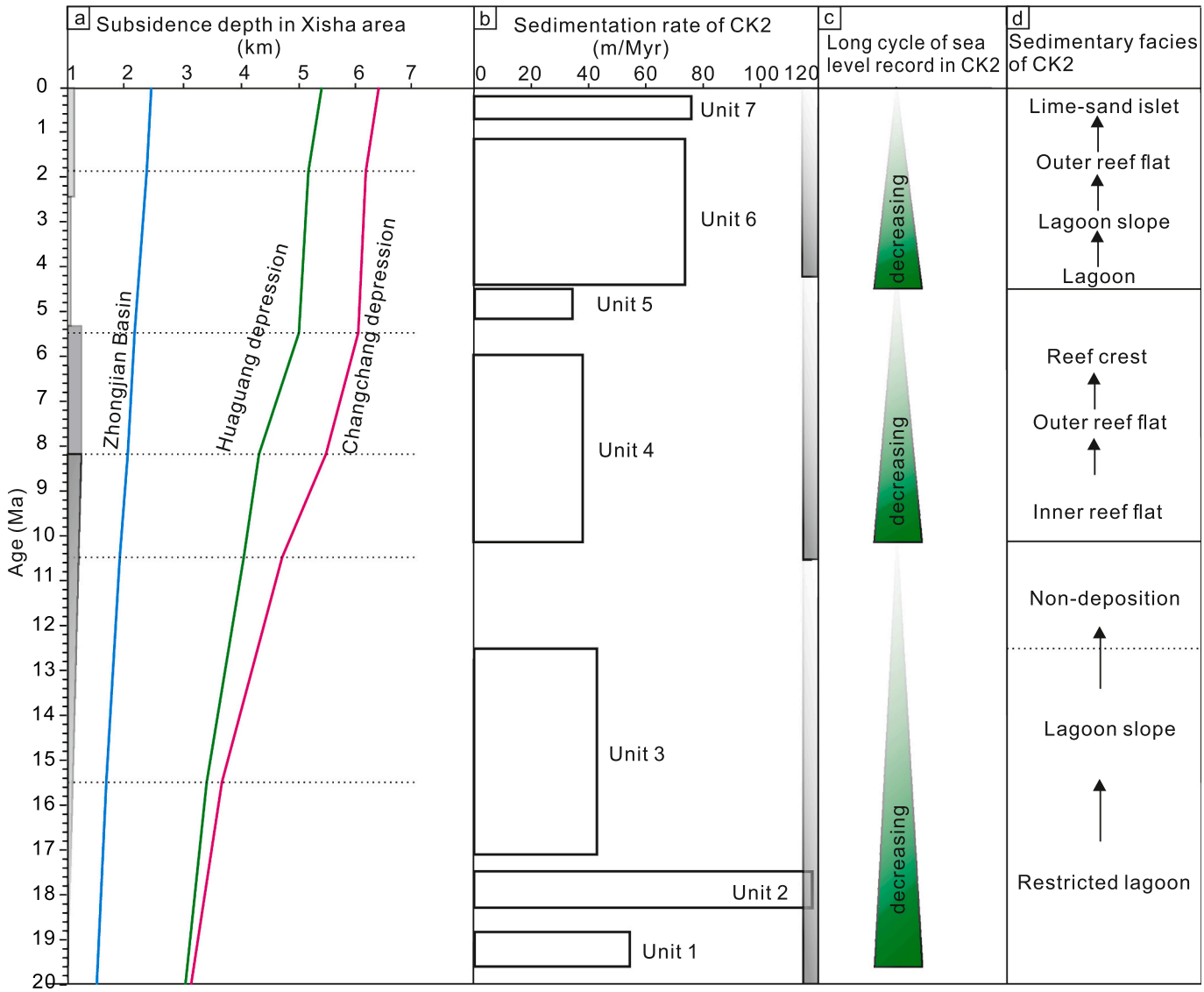

Fig. 8. (a) Tectonic subsidence in Xisha area (Wu et al., 2014), (b) Sedimentation rate of CK2, (c) Long term cycle of sea level fall record in CK2 carbonate $^{87}Sr/^{86}Sr$. (d) Sedimentary facie of CK2.

Miao et al., 2017), resulting in increased input of material with higher $^{87}Sr/^{86}Sr$. The decreased input of material with lower $^{87}Sr/^{86}Sr$ and increased input of material with higher $^{87}Sr/^{86}Sr$ after 15 Ma, should have caused the South China Sea seawater $^{87}Sr/^{86}Sr$ increased fast than before. However, the seawater $^{87}Sr/^{86}Sr$ in the South China Sea, which was recorded by the carbonate strata of CK2 since the Miocene (Fig. 7A), shows that the $^{87}Sr/^{86}Sr$ evolution curve exhibited an inverse trend with the input of source material. That is, the increase rate of $^{87}Sr/^{86}Sr$ before 16.6 Ma was faster than that after 16.6 Ma, and the interruptions and higher $^{87}Sr/^{86}Sr$ ratios of CK2 are inconsistent with the period of increasing terrigenous matter. This suggests that the semi-closed nature of the South China Sea does not affect its seawater $^{87}Sr/^{86}Sr$. In addition, the terrigenous flux into the South China Sea is derived from the Pearl, Red, and Mekong Rivers, of which the $^{87}Sr/^{86}Sr$ ratios are 0.7119, 0.7114, and 0.7119, respectively, similar to the global average river $^{87}Sr/^{86}Sr$ (Palmer and Edmond, 1989; Dia et al., 1992). Collectively, these findings indicate a negligible influence of regional tectonic and climatic changes on seawater $^{87}Sr/^{86}Sr$ in the South China Sea.

5.1.2. Regional tectonic activities and sea level change

Seawater $^{87}Sr/^{86}Sr$ was assimilated by live coral and other organism in the coral reef ecosystem and precipitated in the skeleton and shells when these organisms died. Indeed, seawater $^{87}Sr/^{86}Sr$ was preserved in the biological carbonate after compaction, pressure solution, replacement, and cementation of the skeleton and shells during the diagenesis process. Thus, the evolution of coral reef carbonate $^{87}Sr/^{86}Sr$ is closely related to the vertical development of coral reefs. For example, continuous deposition in the vertical direction produces a continuously increasing $^{87}Sr/^{86}Sr$ curve, such as that observed in Units 1–7. In contrast, non-deposition produces a break in the $^{87}Sr/^{86}Sr$ curve, such as the hiatus that observed between the two increasing $^{87}Sr/^{86}Sr$ units (Fig. 7A).

On the tectonic timescale, tectonic activities and sea level changes may be two of the most important factors impacting coral reef development (Webster et al., 2010; Braithwaite et al., 2004). The main tectonic element in the study area is the Xisha Block, which was separated from the South China continent by the subduction of the paleo-South China Sea during the Eocene-Paleocene, moving further southeast with the expansion of the new South China Sea during the Oligocene. The Xisha Block stopped migrating until the end of late Oligocene (Hall, 2012; Zahirovic et al., 2014). With thermal subsidence after lithospheric cracking, the Xisha-Zhongsha block gradually sank, with nearly all of it

becoming submergedy in the Early Miocene. Consequently, the coral reef system began to develop in the uplift position thereafter (Wu et al., 2014). A previous study by Wu et al. (2014) used seismic data to reconstruct the evolution history of thermal subsidence in Xisha area. They proposed that thermal subsidence is continuous from the Early Miocene to today, and the subsidence rate increased gradually, reaching its peak at 10–8.2 Ma, and nearly ceasing during 5–2.6 Ma (Wu et al., 2014). Thermal subsidence provides initial space for coral reefs to develop upward (Ma et al., 2011). However, the coral reef development recorded by carbonate $^{87}Sr/^{86}Sr$ evolution did not correspond to the thermal subsidence history. The sedimentation rate of CK2, which was calculated based on the Sr-age and thickness of the coral reef carbonate strata after compaction, weathering, and erosion, showed that coral reef carbonate deposited at a high rate during Early Miocene and Pliocene, and at a low rate during Middle Miocene and Late Miocene (Fig. 8b). This inverse relationship suggests that global sea level directly impacts coral reef development. We propose three models to describe the evolution of the coral reef carbonate strata $^{87}Sr/^{86}Sr$ in response to the coupled effects of tectonic subsidence and global sea level changes based on the fact that tectonic activity of the Xisha Block was dominated by subsidence with different rates.

Model 1 hypothesized that the coral reef developed vertically with a sedimentary rate that was 1) higher than the subsidence rate when the global sea level rose; 2) equal to the subsidence rate when the global sea level was invariant; and 3) lower than the subsidence rate when the global sea level fell, and the reduction in range was smaller than the subsidence. This model produces a continuously increasing $^{87}Sr/^{86}Sr$, such as that observed in Units 1–7 (Fig. 7A).

Model 2 hypothesized that the coral reef stops growing or develops in a lateral direction when the rate of sea level fall is equivalent to the subsidence rate. This model describes non-deposition in the vertical direction, thus producing a break in the $^{87}Sr/^{86}Sr$ curve, as exhibited at 841–831 m (Hiatus 1), 731–721 m (Hiatus 2), 526–521 m (Hiatus 3), 361–341 m (Hiatus 4), 316–271 m (Hiatus 5), and 81–61 m (Hiatus 6) (Fig. 7A).

Model 3 hypothesized that the coral reef stops growing or is even destroyed when the sea level decrease rate is greater than the subsidence rate. In this situation, coral reefs may be exposed to weathering and/or erosion, which not only limits vertical reef development (Kendall and Schlager, 1981; Quinn et al., 1991), but also forms a meteoric water vadose zone (with a higher $^{87}Sr/^{86}Sr$) on the surface of the reef carbonate (Melim et al., 2001, 2002). This model reveals a hiatus in the $^{87}Sr/^{86}Sr$ curve or a higher $^{87}Sr/^{86}Sr$ interval in the reef carbonate sequence, with the former exhibiting as Hiatus 1–6, and the latter appearing at 672–616 m (Interval I), 601–578 m (Interval II), 521–481 m (Interval III), 426–411 m (Interval IV), and 201–152 m (Interval V) (Fig. 7A).

Of note, we did not consider the drowning factor, which leads to the demise of coral reef, as the drowning event is typically caused by a rapid sea-level rise on 10^2–10^3 -year time scales (Buddemeier and Smith, 1988; Clark et al., 1995; Webster et al., 2004; Abbey et al., 2011), which can be ignored under the 10^6–10^7 year time scale evaluated in this study. The three models clearly indicate that the thermal subsidence provided initial advantages for coral reef development, while global sea level rise resulted in a positive superposition on the coral reef development, whereas sea level fall resulted in a negative superposition on coral reef development. Thus, the continuously increasing $^{87}Sr/^{86}Sr$ of CK2 is controlled by the coupled effects of tectonic subsidence and sea level changes. A hiatus and higher $^{87}Sr/^{86}Sr$ interval in the $^{87}Sr/^{86}Sr$ curve are dominated only by a fall in sea level.

5.1.3. Evaluate the hypothesis

Based on the discussion above, we proposed a hypothesis that the hiatus and higher $^{87}Sr/^{86}Sr$ of CK2 coral reef carbonate were produced by a fall in sea level. We tested this hypothesis through investigation of petrological features. In periods during which the sea level is low, shallow carbonate typically forms on an exposed surface which is characterized by karst, fracture, and corrosion cavern accompanied by reddish-brown Fe oxides after weathering and leaching (Lincoln and Schlanger, 1991; Sano, 2006; Lewis et al., 2012). The exposed surface is an important indicator of sea level fall, which appeared at depths of 840–830 (j), 671–611 (i), 526–518 (h), 426 (g), 361–341 (f), 312.5–294 (e), 196–190 (d), 133–121 (c), 90–60 (b), and 32–34 m (a) in the CK2 carbonate strata (Fig. 4E and the supplement material 1). At these intervals, the exposed surfaces b, e, f, and j showed an $^{87}Sr/^{86}Sr$ hiatus and correspond to Hiatus periods 6, 5, 4, 3, and 1, respectively. The exposed surfaces d, g, h, and i showed higher $^{87}Sr/^{86}Sr$ intervals and correspond to intervals V, III, II, and I, respectively (Fig. 7A). These corresponding values verified the hypothesis that the hiatus and higher $^{87}Sr/^{86}Sr$ interval in the $^{87}Sr/^{86}Sr$ curve of the CK2 core were produced by a decrease in sea level. However, caution should be used when applying this model, as not all decreases in sea level can be recorded in the $^{87}Sr/^{86}Sr$ curve. We also analyzed the $^{87}Sr/^{86}Sr$ at the interval of the exposed surface in CK2, and found that the $^{87}Sr/^{86}Sr$ ratios were only notably increased at depths of 521–481, 317–309, and 311–191 m, whereas other intervals were similar to the adjacent normal strata within the error range (Table 2 and Fig. 7A). This may be due to a lack of vadose zones with active geochemical processes during the periods of low sea levels, which did not provide fluids with a higher $^{87}Sr/^{86}Sr$.

The element content and ratio can also be used to evaluate the hypothesis. Previous studies have shown that external fluid, such as pore water, meteoric water, dolomite fluid, and hydrothermal fluid, can react with carbonate to change the $^{87}Sr/^{86}Sr$ (Brand and Veizer, 1980; Vahrenkamp et al., 1988; Kaufman et al., 1993; Ren and Jones, 2017). Moreover, carbonate altered in open systems during a lowstand may lead to a lower Sr/Ca and higher Sr content as meteoric water generally has a higher Mn content, lower Sr content, and higher $^{87}Sr/^{86}Sr$ (Brand and Veizer, 1980). As shown in Fig. 5, intervals I (672–616 m), III (521–491 m), and IV (423–414 m) were characterized by lower Sr/Ca and Sr contents, while III (521–491 m), IV (423–414 m), and V (192.5–161 m) were characterized by higher Mn/Sr and Mn contents. These intervals are in accord with the higher $^{87}Sr/^{86}Sr$ of CK2, indicating that the higher $^{87}Sr/^{86}Sr$ may result from the meteoric water alterations during a sea level lowstand.

5.2. Global sea level changes record by coral reef carbonate $^{87}Sr/^{86}Sr$

5.2.1. Long term trend of sea level recorded by the continuous $^{87}Sr/^{86}Sr$ of CK2

The continuously increasing $^{87}Sr/^{86}Sr$ of Units 1–7 (Fig. 7A) is controlled by the coupled effects of tectonic subsidence and sea level changes according to model 1. A continuous increase in the $^{87}Sr/^{86}Sr$ of the CK2 coral reef carbonate sequence indicates the gradual upward growth of coral reefs as the relative sea levels rise in Xisha area. The relative sea levels change in Xisha area are influenced by the rate of global sea level change and regional tectonic subsidence rate. The sedimentation rate of Units 1–7 showing three long term trends, namely the decreasing trend from Unit 1, 2 to 3 during 19.6–10.19 Ma, the lowest trend as Unit 4 and 5 during 10.19–4.45 Ma, and the highest trend as Unit 6 and 7 during 4.45–0.74 Ma (Fig. 8b).

The decreasing sedimentation rate of CK2 suggests a decreasing relative sea level in Xisha area during 19.6–10.19 Ma, which are supported by the sedimentary facies, from restricted lagoon to lagoon slope to no deposition (Fig. 8d). However, the regional tectonic subsidence rate continuously increased during this interval (Wu et al., 2014). Therefore, a decreasing trend in global sea level is needed to meet the decreasing relative sea level in Xisha area. Similarly, a long term decrease in global sea level was also recorded in the Atlantic (Haq et al., 1987) and Pacific (Quinn et al., 1991; Lincoln and Schlanger, 1991; Ohde and Elderfield, 1992) (Fig. 10d). The lowest sedimentation rate during 10.19–4.45 Ma corresponded to the highest tectonic subsidence rate, suggesting a lowstand of global sea level. Although the

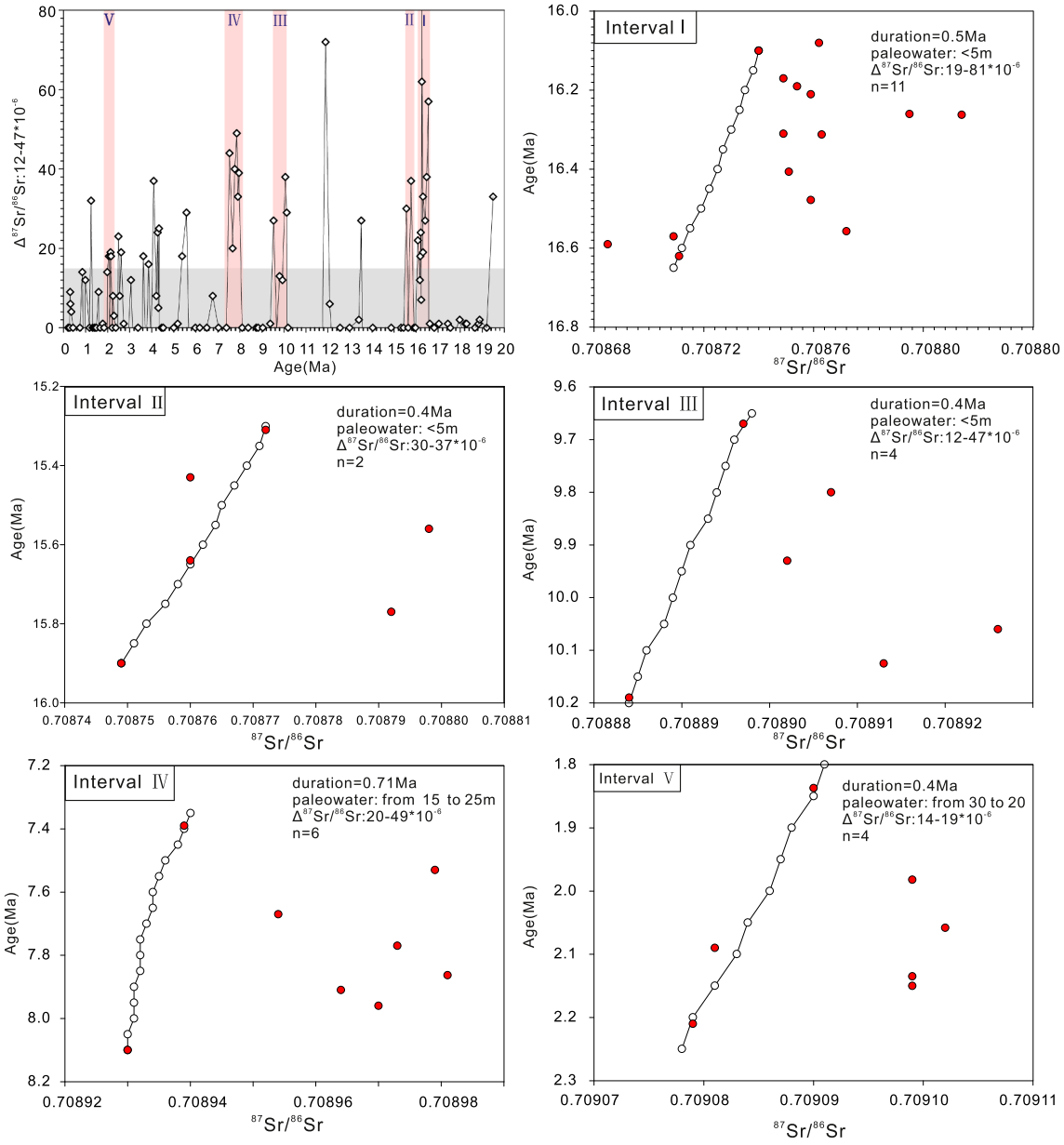

Fig. 9. Shift of $^{87}Sr/^{86}Sr$ during Interval I, II, III, IV, V.

sedimentation rate during 10.19–4.45 Ma did not overly change, the sedimentary facies changed from an inner to outer reef flat, and subsequently, to a reef crest, thus, indicating a decrease in the relative sea level in the Xisha area. These findings suggest a decreasing trend in the global sea level as the tectonic subsidence rate exhibited negligible changes during this interval. The second decreasing trend in the global sea level was also recorded in the Pacific (Quinn et al., 1991; Lincoln and Schlanger, 1991; Ohde and Elderfield, 1992; Miller et al., 2005) (Fig. 10d). Although the highest sedimentation rate during 4.45–0.74 Ma (Fig. 8b) corresponding to the lowest tectonic subsidence rate, indicates a highstand global sea level, the sedimentary facies changed from lagoon to lagoon slope to outer reef flat to lime-sand islet, suggesting a decreasing relative sea level in the Xisha area. Combined with the fact that the tectonic subsidence rate increased from 5.5–1.9 Ma to 1.9–0 Ma, we can conclude that global sea level exhibited a decreasing trend during 4.45–0.74 Ma, which is supported by the sea level change in Pacific (Miller et al., 2005) and Atlantic (Haq et al., 1987) (Fig. 10d).

5.2.2. *Sea level fall recorded by the abnormal $^{87}Sr/^{86}Sr$ of CK2*

According to model 2 and 3, the $^{87}Sr/^{86}Sr$ hiatus and higher $^{87}Sr/^{86}Sr$ of CK2 are produced by the drop in global sea level. The coral reef carbonate strata $^{87}Sr/^{86}Sr$ ratios of CK2 contained six hiatuses and five higher $^{87}Sr/^{86}Sr$ intervals (Fig. 7A), suggesting that 11 sea level fall events occurred from the Early Miocene to the Pleistocene. We constrained the age based on strontium isotope stratigraphy (Fig. 7B), which was described in detail in Section 4.5 and the supplementary material 2. The six hiatuses indicated that the sea level decreased during 18.83–18.29, 17.44–17.12, 12.55–10.19, 5.98–5.18, 4.45, and 1.18–0.74 Ma, while the five higher $^{87}Sr/^{86}Sr$ intervals suggested that the sea level decreased during 16.62–16.1, 15.64–15.31, 10.19–9.67, 8.1–7.39, and 1.58–1.5 Ma. At low sea level, some of the coral reef carbonate may have been exposed to erosion which impacts the reconstruction precision, thus, the time at which the sea level began to fall, as reconstructed here, may represent the earliest possible period of sea level fall, while the ending time represents the latest period of sea level fall. In models 2 and 3, the sea level fall can be recorded in the coral reef carbonate strata $^{87}Sr/^{86}Sr$ only when the range of the sea level decrease

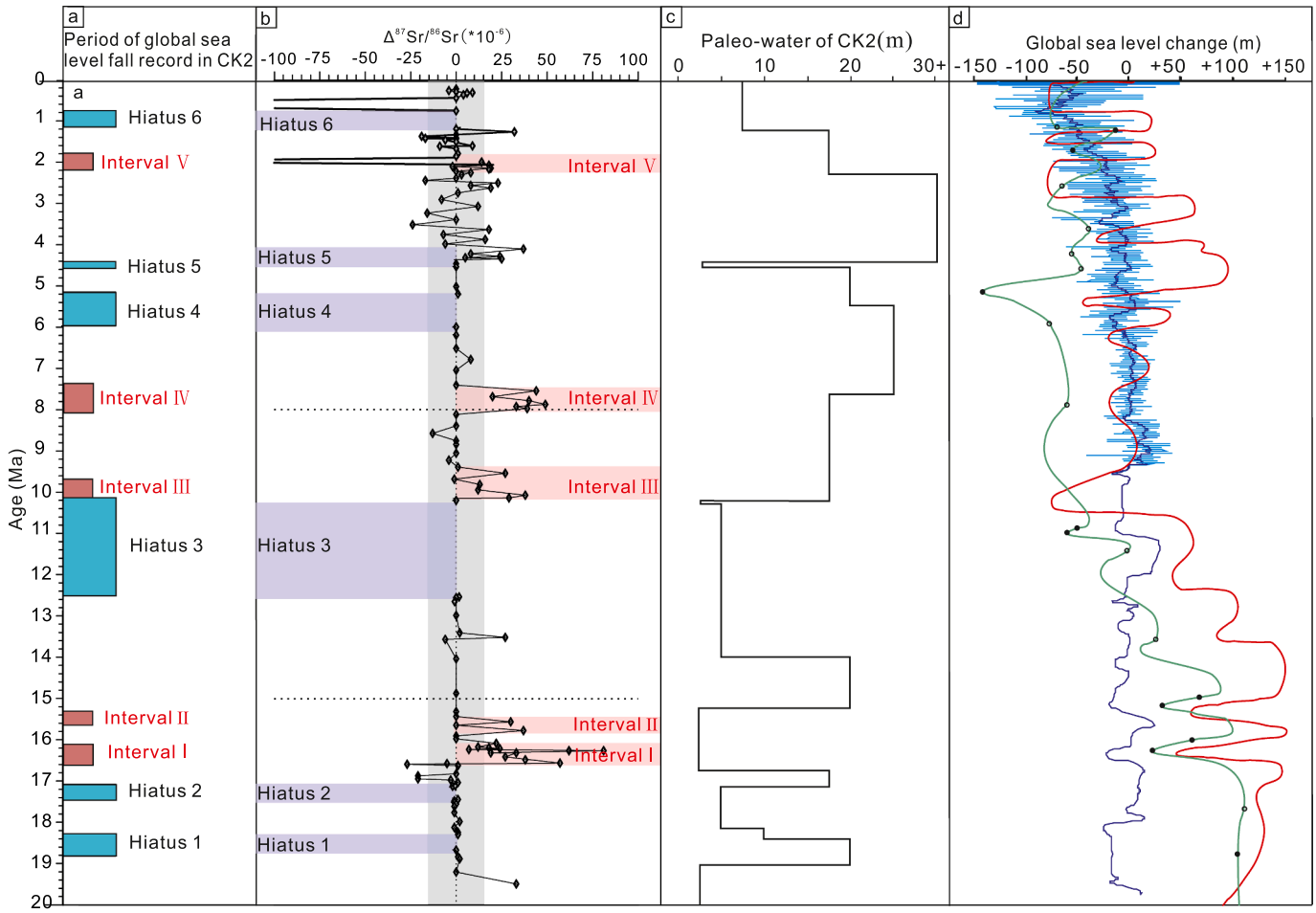

Fig. 10. (a) Sea level falls recorded by the coral reef carbonate $^{87}Sr/^{86}Sr$ of CK2. (b) $\Delta^{87}Sr/^{86}Sr$" ($^{87}Sr/^{86}Sr_{carbonate}$ - $^{87}Sr/^{86}Sr_{seawater}$) x 10^{-6} of CK2. (c) Paleo-water depth of CK2 (Li et al., 2020, 2021). (c) Global sea level fluctuations curve. (Red are derived from passive continental margin sequence in the Atlantic (Haq et al., 1987); Blue are derived from New Jersey craton basin strata and foraminifera $\delta^{18}O$ in global ocean (Miller et al., 2005); Green are derived from Kita-Daito-jima Atoll in Philippine Sea (Ohde and Elderfield, 1992) and Enewetak Atoll in Pacific (Lincoln and Schlanger, 1991). (For interpretation of the references to colour in this figure legend, the reader is referred to the web version of this article.)

is equal to or larger than the tectonic subsidence rate. However, we were unable to obtain accurate data on the ranges of sea level decreases during these periods, as the detailed tectonic subsidence rate of the Xisha Block had not been evaluated. Nevertheless, the three cycles of global sea level decreases suggestd that the greatest decreases in sea level occurred at 10.19, 4.45, and 0.74 Ma. Moreover, the long period of non-deposition, and lowest sedimentation rate without an obvious change in tectonic subsidence rate during the Middle Miocene, indicated that the sea level reached a minimum at 10.19 Ma. This prediction is consistent with the sea level curve reported by Haq et al. (1987).

The eleven sea level fall records in the coral reef carbonate strata $^{87}Sr/^{86}Sr$ from CK2 were also observed in the Atlantic (Haq et al., 1987), global ocean (Miller et al., 200), Pacific (Quinn et al., 1991; Lincoln and Schlanger, 1991; Ohde and Elderfield, 1992) (Fig. 10d). Sea level decreases during 16.62–16.1, 15.64–15.31, 12.55–9.67, 5.98–5.18, and 4.45 Ma were recorded in all three records above. However, sea level falls during 17.44–17.12 Ma were only recorded in the Atlantic, during 8.1–7.39 and 1.5 Ma in the Atlantic and global ocean, and during 1.18–0.74 Ma in the Pacific and global ocean. Meanwhile, the sea level decrease at 18.83–18.29 Ma was not previously recorded. These results suggest that hiatuses and higher $^{87}Sr/^{86}Sr$ intervals in the coral reef carbonate strata are reliable indicators of sea level fall. The sea level records in Yongle Atoll in the South China Sea, Enewetak Atoll in central Pacific Ocean and Kita-Daito-jima Atoll in Philipine Sea, and Yongle Atoll record are more complete, possibly due to the different deposition rates, as the thicknesses of the Enewetak Atoll and Kita-Daito-jima Atoll (<400 m) have been significantly lower than that of the Yongle Atoll (873.55 m) since the Miocene.

5.2.3. *Constrain the shift of $^{87}Sr/^{86}Sr$ during sea level change*

We tried to constrain the shift of $^{87}Sr/^{86}Sr$ during sea level fall by comparing changes in $^{87}Sr/^{86}Sr$ and paleo-water depth at the same period. Coral algal assemblages (CAASs) in shallow water carbonate are useful indicator of reconstructed paleo-water (Williamson et al., 2015; Porzio et al., 2018;Coletti et al., 2019; Coletti and Basso, 2020). Indeed, the evolutionary history of paleo-water was reconstructed by Li et al. (2020) and Li et al. (2021) based on CAASs. The detailed information regarding the shift of $^{87}Sr/^{86}Sr$, CAASs, paleo-water depth, and global sea level changes, for the six $^{87}Sr/^{86}Sr$ hiatuses and five higher $^{87}Sr/^{86}Sr$ intervals have been presented in the Supplementary material 2.

Hiatus 1, 4 and 6 recorded the fall in sea level during 18.83–18.29 Ma, 5.98–5.18 Ma and 1.18–0.14 Ma, respectively, with corresponding shift of $^{87}Sr/^{86}Sr$ by 40×10^{-6}, 42×10^{-6} and 22×10^{-6}. CAASs during these intervals all indicate paleo-water changes from a deep to shallow depth, with all of them depositing in a relatively deep water sedimentary environment (>10 m). Additionally, Hiatus 5 recorded the decrease in sea level during 4.45–3.8 Ma, with a 14×10^{-6} $^{87}Sr/^{86}Sr$ shift. The CAASs during this interval indicate a very shallow paleo-water (5 m). Hiatus 2 and 3 recorded the fall in sea level during 17.44–17.12 Ma and 12.55–10.19 Ma, with $^{87}Sr/^{86}Sr$ shift by 28×10^{-6} and 58×10^{-6},

respectively. The CAASs during these intervals indicate a relative shallow paleo-water (10 m).

We used "$\Delta^{87}Sr/^{86}Sr$" ($(^{87}Sr/^{86}Sr_{carbonate}-^{87}Sr/^{86}Sr_{seawater})*10^6$) (Edwards et al., 2015) to constrain the $^{87}Sr/^{86}Sr$ shift at the higher $^{87}Sr/^{86}Sr$ intervals. Interval I, II, III and V record the fall in sea level during 16.62–16.1 Ma, 15.9–15.43 Ma, 10.19–9.67 Ma and 2.2–1.8 Ma, with $\Delta^{87}Sr/^{86}Sr$ of 19–81, 30–37, 12–47 and 14–19, respectively (Fig. 9). The CAASs during these intervals indicate a very shallow paleo-water (5 m).

Based on the discussion above, we can conclude that higher $^{87}Sr/^{86}Sr$ generally correlated with low sea level (<5 m), while a hiatus in $^{87}Sr/^{86}Sr$ was often produced when the sea level changed from deep to shallow. Specifically, the $^{87}Sr/^{86}Sr$ shift are very low during 4.45–3.8 Ma, 2.2–1.8 Ma and 1.18–0.14 Ma, which may be caused by the slow rate of seawater $^{87}Sr/^{86}Sr$ change.

6. Conclusion

A total of 160 coral reef carbonate strata $^{87}Sr/^{86}Sr$ ratios and the petrology from CK2 at the Yongle Atoll in the South China Sea were analyzed in this study. Conclusions are as follows:

(1) Ten exposed surfaces were identified based on their petrologic features, with exposed surfaces appearing at 32–34, 60–90, 121–133, 190–196, 294–312.5, 341–361, 426, and 518–526 m.
(2) The Mn content, Sr content, Mn/Sr, Sr/Ca, $\delta^{18}O$ values, and correlations between these proxies were used to constrain the degree of alteration. The results suggested that most coral reef carbonate of the CK2 core preserved the original seawater $^{87}Sr/^{86}Sr$ except at intervals of 672–616, 596–575, 521–491, 423–414, and 192.5–161 m, where $^{87}Sr/^{86}Sr$ was higher than the adjacent strata.
(3) The continuously increased $^{87}Sr/^{86}Sr$ curve of CK2 was divided into seven units by six $^{87}Sr/^{86}Sr$ hiatuses. The inconsistency between the sedimentation rate of the seven units of the CK2 core and tectonic subsidence of the Xisha area suggest that the continuously increasing $^{87}Sr/^{86}Sr$ of CK2 is controlled by the coupled effects of tectonic subsidence and sea level changes. In contrast, the hiatus and higher $^{87}Sr/^{86}Sr$ interval in the $^{87}Sr/^{86}Sr$ curve are dominated only by sea level fall. The higher $^{87}Sr/^{86}Sr$ usually produced during low sea level (<5 m), $^{87}Sr/^{86}Sr$ hiatus usually produced when sea level changed from deep to shallow.
(4) The consistency of the exposed surface and abnormal $^{87}Sr/^{86}Sr$ ratios support that the hiatus and higher $^{87}Sr/^{86}Sr$ interval in the coral reef carbonate strata $^{87}Sr/^{86}Sr$ curve can be used as an effective indicator of sea level fall.
(5) Based on the $^{87}Sr/^{86}Sr$ hiatus and higher $^{87}Sr/^{86}Sr$ intervals, we detected 11 sea level fall events. The age are constrained based on strontium isotope stratigraphy. Sea level fall occurred during 18.83–18.29, 17.44–17.12, 16.62–16.1, 15.64–15.31, 12.55–10.19, 10.19–9.67, 8.1–7.39, 5.98–5.18, 4.45, 1.58–1.5, and 1.18–0.74 Ma. .
(6) Three long term decreased cycle in sea level were reconstructed based on continuous increasing $^{87}Sr/^{86}Sr$. The three dramatic regression occurred at 19.6–10.19, 10.19–4.45, 4.45–0.74 Ma.

Data availability

The data used in this paper have been deposited in a general data repository; and they are available from the link (doi: https://doi.org/10.6084/m9.figshare.19160558).

Declaration of Competing Interest

This manuscript has not been published or presented elsewhere in part or in entirety and is not under consideration by another journal. We have read and understood your journal's policies, and we believe that neither the manuscript nor the study violates any of these. There are no conflicts of interest to declare.

Acknowledgments

This work was financially supported by the National Natural Science Foundation of China (Grant Nos. 42030502 and 42090041) and Guangxi Scientific projects (Nos. AD17129063 and AA17204074).

Appendix A. Supplementary data

Supplementary data to this article can be found online at https://doi.org/10.1016/j.margeo.2022.106758.

References

Abbey, E., Webster, J.M., Braga, J.C., et al., 2011. Variation in deglacial coralgal assemblages and their paleoenvironmental significance: IODP expedition 310, "Tahiti Sea Level". Glob. Planet. Chang. 76, 1–15. https://doi.org/10.1016/j.gloplacha.2010.11.005.

An, Z.S., Kutzbach, J.E., Prell, W.L., et al., 2001. Evolution of Asian monsoon and phased uplift of the Himalaya-Tibetan plateau since Late Miocene times. Nature 411, 62–66.

Braithwaite, C.J., Dalmasso, H., Gilmour, et al., 2004. The Great Barrier Reef: the chronological record from a new Borehole. J. Sediment. Res. 74, 298–310. https://doi.org/10.1306/091603740298.

Brand, U., Veizer, J., 1980. Chemical diagenesis of a multicomponent carbonate system; 1, trace elements. J. Sediment. Petrol. 50, 1219–1236. https://doi.org/10.1306/212F7BB7-2B24-11D7-86 48000102C1865D.

Buddemeier, R.W., Smith, S.V., 1988. Coral reef growth in an era of rapidly rising sea level: predictions and suggestions for long-term research. Coral Reefs 7, 51–56. https://doi.org/10.1007/BF00301982.

Burke, W.H., Denison, R.E., Hetherington, E.A., et al., 1982. Variation of seawater $^{87}Sr/^{86}Sr$ throughout Phanerozoic time. Geology 10, 516–519. https://doi.org/10.1130/0091-7613(1982)102.0.CO;2.

Camoin, G.F., Ebren, P., Eisenhauer, A., et al., 2001. A 300 000-yr coral reef record of sea level changes, Mururoa atoll (Tuamotu archipelago, French Polynesia). Palaeogeogr. Palaeoclimatol. Palaeoecol. 175, 325–341. https://doi.org/10.1016/S0031-0182(01)00378-9.

Clark, P.U., Blanchon, P., Shaw, J., 1995. Reef drowning during the last deglaciation: evidence for catastrophic sea-level rise and ice-sheet collapse. Geology 23, 957.

Coletti, G., Basso, D., 2020. Coralline algae as depth indicators in the Miocene carbonates of the Eratosthenes Seamount (ODP Leg 160, Hole 966F). Geobios 60, 29–46.

Coletti, G., Basso, D., Betzler, C., Robertson, A.H.F., Spezzaferri, S., 2019. Environmental evolution and geological significance of the Miocene carbonates of the Eratosthenes Seamount (ODP Leg 160). Palaeogeogr. Palaeoclimatol. Palaeoecol. 530, 217–235.

Depaolo, D.J., Ingram, B.L., 1985. High-resolution stratigraphy with strontium isotopes. Science 227, 938–941. https://doi.org/10.1126/science.227.4689.938.

Derry, L.A., Keto, L.S., Jacobsen, S.B., et al., 1989. Sr isotopic variations in Upper Proterozoic carbonates from Svalbard and East Greenland. Geochim. Cosmochim. Acta 53, 2331–2339. https://doi.org/10.1016/0016-7037(89)90355-4.

Dia, A.N., Cohen, A.S., O'Nions, R.K., et al., 1992. Seawater Sr isotope variation over the past 300 kyr and influence of global climate cycles. Nature 356, 786–788. https://doi.org/10.1038/356786a0.

Edwards, C.T., Saltzman, M.R., Leslie, S.A., et al., 2015. Strontium isotope ($^{87}Sr/^{86}Sr$) stratigraphy of ordovician bulk carbonate: implications for preservation of primary seawater values. Geol. Soc. Am. Bull. 127, 1275–1289. https://doi.org/10.1130/B31149.1.

Fairbanks, R.G., 1989. A 17,000-year glacio-eustatic sea level record: influence of glacial melting rates on the Younger Dryas event and deep-ocean circulation. Nature 342, 637–642. https://doi.org/10.1038/342637a0.

Fan, T., Yu, K., Zhao, J., et al., 2020. Strontium isotope stratigraphy and paleomagnetic age constraints on the evolution history of coral reef islands, northern South China Sea. Geol. Soc. Am. Bull. 132, 803–816. https://doi.org/10.1130/B35088.1.

Fyhn, M.B.W., Boldreel Lars, O., Nielsen Lars, H., 2009. Geological development of the Central and South Vietnamese margin: implications for the establishment of the South China Sea, Indochinese escape tectonics and Cenozoic volcanism. Tectonophysics 478, 184–214.

Fyhn, M.B.W., Boldreel, L.O., Nielsen, L.H., et al., 2013. Carbonate platform growth and demise offshore Central Vietnam: effects of Early Miocene transgression and subsequent onshore uplift. J. Asian Earth Sci. 76, 152–168. https://doi.org/10.1016/j.jseaes.2013.02.023.

Gasson, E., Siddall, M., Lunt, D.J., et al., 2012. Exploring uncertainties in the relationship between temperature, ice volume, and sea level over the past 50 million years. Rev. Geophys. 50 https://doi.org/10.1029/2011RG000358.

Guo, Z.T., Ruddiman, William F., et al., 2002. Onset of Asian desertification by 22 Myr ago inferred from loess deposits in China. Nature 416, 159–163. https://doi.org/10.1038/416159a.

Hall, R., 2012. Late Jurassic–Cenozoic reconstructions of the Indonesian region and the Indian Ocean. Tectonophysics 11, 1–41. https://doi.org/10.1016/j.tecto.2012.04.021.

Haq, B.U., Hardenbol, J., Vail, P.R., 1987. Chronology of fluctuating sea levels since the triassic. Science 235, 1156–1167. https://doi.org/10.1126/science.235.4793.1156.
Hess, J., Bender, M.L., Schilling, J.G., 1986. Evolution of the ratio of strontium-87 to strontium-86 in seawater from cretaceous to present. Science 231 (4741), 979–984. https://doi.org/10.1126/science.231.4741.979.
Hodell, D.A., Woodruff, F., 1994. Variations in the strontium isotopic ratio of seawater during the Miocene: stratigraphic and geochemical implications. Paleoceanography 9, 405–426. https://doi.org/10.1029/94PA00292.
Hodell, D.A., Elmstrom, K.M., Kennett, J.P., 1986. Latest Miocene benthic $\delta^{18}O$ changes, global ice volume, sea level and the 'messinian salinity crisis'. Nature 320, 411–414. https://doi.org/10.1038/320411a0.
Hodell, D.A., Mead, G.A., Mueller, P.A., 1990. Variation in the strontium isotopic composition of seawater (8 Ma to present): implications for chemical weathering rates and dissolved fluxes to the oceans. Chem. Geol. 80, 291–307. https://doi.org/10.1016/0168-9622(90)90011-Z.
Huang, X., Niu, Y., Xu, Y., et al., 2013. Geochronology and geochemistry of Cenozoic basalts from eastern Guangdong, SE china: constraints on the lithosphere evolution beneath the northern margin of the south china sea. Contrib. Mineral. Petrol. 165, 437–455. https://doi.org/10.1007/s00410-012-0816-7.
Jiang, G., Shi, X., Zhang, S., et al., 2011. Stratigraphy and paleogeography of the Ediacaran Doushantuo Formation (ca. 635–551 Ma) in South China. Gondwana Res. 19, 831–849. https://doi.org/10.1016/j.gr.2011.01.006.
Jiang, W., Yu, K., Fan, T., et al., 2019. Coral reef carbonate record of the Pliocene-Pleistocene climate transition from an atoll in the South China Sea. Mar. Geol. 411, 88–97. https://doi.org/10.1016/j.margeo.2019.02.006.
John, C.M., Karner, G.D., Mutti, M., 2004. $\delta^{18}O$ and Marion Plateau backstripping: combining two approaches to constrain late middle Miocene eustatic amplitude. Geology 32, 829–832. https://doi.org/10.1130/G20580.1.
Kaufman, A.J., Knoll, A.H., Awramik, S.M., 1992. Biostratigraphic and chemostratigraphic correlation of Neoproterozoic sedimentary successions: upper Tindir Group, northwestern Canada, as a test case. Geology 20, 181. https://doi.org/10.1130/0091-7613(1992)020<0181:BACCON>2.3.CACCON>2.3.CO;2.
Kaufman, A.J., Jacobsen, S.B., Knoll, A.H., 1993. The vendian record of sr and c isotopic variations in seawater: implications for tectonics and paleoclimate. Earth Planet. Sci. Lett. 120, 409–430. https://doi.org/10.1016/0012-821X(93)90254-7.
Kendall, C., Schlager, W., 1981. Carbonates and relative changes in sea level. Mar. Geol. 44, 181–212.
Korte, C., Kozur, H.W., Bruckschen, P., et al., 2003. Strontium isotope evolution of Late Permian and Triassic seawater. Geochim. Cosmochim. Acta 67, 47–62. https://doi.org/10.1016/S0016-7037(02)01035-9.
Lambeck, K., Chappell, J., 2001. Sea level change through the last glacial cycle. Science 292, 679–686. https://www.jstor.org/stable/3083538.
Lambeck, K., Purcell, A., 2005. Sea-level change in the Mediterranean Sea since the LGM: model predictions for tectonically stable areas. Quat. Sci. Rev. 24, 1969–1988. https://doi.org/10.1016/j.quascirev.2004.06.025.
Lewis, S.E., Raphael, A.J.W., Webster, J.M., et al., 2012. Development of an inshore fringing coral reef using textural, compositional and stratigraphic data from Magnetic Island, Great Barrier Reef, Australia. Mar. Geol. 299-302, 18–32. https://doi.org/10.1016/j.margeo.2012.01.003.
Li, D., Shields-Zhou, G.A., Ling, H.F., et al., 2011a. Dissolution methods for strontium isotope stratigraphy: guidelines for the use of bulk carbonate and phosphorite rocks. Chem. Geol. 290, 133–144. https://doi.org/10.1016/j.chemgeo.2011.09.004.
Li, G.J., Pettke, T., Chen, J., 2011b. Increasing Nd isotopic ratio of Asian dust indicates progressive uplift of the north Tibetan Plateau since the middle Miocene. Geology 39, 199–202.
Li, Y., Yu, K., Bian, L., et al., 2020. Paleo-water depth variations since the Pliocene as recorded by coralline algae in the South China Sea. Palaeogeogr. Palaeoclimatol. Palaeoecol. 562, 110107. https://doi.org/10.1016/j.palaeo.2020.110107.
Li, Y., Yu, K., Bian, L., et al., 2021. Coralline algal assemblages record Miocene sea-level changes in the South China Sea. Palaeogeogr. Palaeoclimatol. Palaeoecol. 584, 110673. https://doi.org/10.1016/j.palaeo.2021.110673.
Lincoln, J.M., Schlanger, S.O., 1991. Atoll stratigraphy as a record of sea level change: problems and prospects. J. Geophys. Res. Solid Earth 96, 6727–6752. https://doi.org/10.1029/90JB00601.
Liu, Z., Colin, C., Huang, W., et al., 2007. Climatic and tectonic controls on weathering in south China and Indochina Peninsula: clay mineralogical and geochemical investigations from the Pearl, Red, and Mekong drainage basins. Geochem. Geophys. Geosyst. 8, Q05005 https://doi.org/10.1029/2006GC001490.
Liu, Z., Zhao, Y., Colin, C., et al., 2016. Source-to-sink transport processes of fluvial sediments in the south china sea. Earth Sci. Rev. 153, 238–273.
Ludwig, K.R., Halley, R.B., Simmons, K.R., et al., 1988. Strontium-isotope stratigraphy of Enewetak atoll. Geology 16, 173–177. https://doi.org/10.1130/0091-7613(1988)016<0173:SISOEA>2.3.CO;2.
Ma, Y., Wu, S., Fuliang, L., et al., 2011. Seismic characteristics and development of the Xisha carbonate platforms, northern margin of the South China Sea. J. Asian Earth Sci. 40, 770–783. https://doi.org/10.1016/j.jseaes.2010.11.003.
Marenco, P.J., Corsetti, F.A., Kaufman, A.J., et al., 2008. Environmental and diagenetic variations in carbonate associated sulfate: an investigation of CAS in the Lower Triassic of the western USA. Geochim. Cosmochim. Acta 72, 1570–1582. https://doi.org/10.1016/j.gca.2007.10.033.
McArthur, J.M., Howarth, R.J., Bailey, T.R., 2001. Strontium isotope stratigraphy: LOWESS version 3: best fit to the marine Sr-isotope curve for 0-509 Ma and accompanying look-up table for deriving numerical age. J. Geol. 109, 155–170. https://doi.org/10.1086/319243.
McArthur, J.M., Steuber, T., Page, K.N., et al., 2016. Sr-isotope stratigraphy: assigning time in the campanian, pliensbachian, toarcian, and valanginian. J. Geol. 124, 569–586. https://doi.org/10.1086/687395.
Melim, L.A., Swart, P.K., Maliva, R.G., 2001. Meteoric and Marine-Burial Diagenesis in the Subsurface of Great Bahama Bank. SEPM, pp. 137–161.
Melim, L.A., Westphal, H., Swart, P.K., et al., 2002. Questioning carbonate diagenetic paradigms: evidence from the Neogene of the Bahamas. Mar. Geol. 185, 27–53. https://doi.org/10.1016/s0025-3227(01)00289-4.
Menier, D., Pierson, B., Chalabi, A., et al., 2014. Morphological indicators of structural control, relative sea-level fluctuations and platform drowning on present-day and Miocene carbonate platforms. Mar. Pet. Geol. 58, 776–788. https://doi.org/10.1016/j.marpetgeo.2014.01.016.
Miao, Y., Warny, S., Clift, P.D., et al., 2017. Evidence of continuous Asian summer monsoon weakening as a response to global cooling over the last 8 Ma. Gondwana Res. 52, 48–58.
Miller, K.G., Kominz, M.A., Browning, J.V., et al., 2005. The Phanerozoic record of global sea-level change. Science 310, 1293–1298. https://doi.org/10.1126/science.1116412.
Milne, G.A., Gehrels, W.R., Hughes, C.W., et al., 2009. Identifying the causes of sea-level change. Nat. Geosci. 2, 471–478. https://doi.org/10.1038/ngeo544.
Ohde, S., Elderfield, H., 1992. Strontium isotope stratigraphy of Kita-daito-jima Atoll, North Philippine Sea: implications for Neogene sea-level change and tectonic history. Earth Planet. Sci. Lett. 113, 473–486. https://doi.org/10.1016/0012-821X(92)90125-F.
Palmer, M.R., Edmond, J.M., 1989. The strontium isotope budget of the modern ocean. Earth Planet. Sci. Lett. 92, 11–26.
Peltier, W.R., Fairbanks, R.G., 2006. Global glacial ice volume and Last Glacial Maximum duration from an extended Barbados sea level record. Quat. Sci. Rev. 25, 3322–3337. https://doi.org/10.1016/j.quascirev.2006.04.010.
Peterman, Z.E., Hedge, C.E., Tourtelot, H.A., 1970. Isotopic composition of strontium in sea water throughout Phanerozoic time. Geochim. Cosmochim. Acta 34, 105–120. https://doi.org/10.1016/0016-7037(70)90154-7.
Porzio, L., Buia, M.C., Lorenti, M., Vitale, E., Amitrano, C., Arena, C., 2018. Ecophysiological response of Jania rubens (Corallinaceae) to ocean acidification. Rend. Lincei-Sci. Fisiche Nat. 29, 543–546.
Prokoph, A., Shields, G.A., Veizer, J., 2008. Compilation and time-series analysis of a marine carbonate $\delta^{18}O$, $\delta^{13}C$, $^{87}Sr/^{86}Sr$ and $\delta^{34}S$ database through Earth history. Earth Sci. Rev. 87, 113–133. https://doi.org/10.1016/j.earscirev.2007.12.003.
Quinn, T.M., Lohmann, K.C., Halliday, A.N., 1991. Sr Isotopic variation in shallow water carbonate sequences: stratigraphic, chronostratographic, and eustatic implications of the record at Enewetak atoll. Paleoceanography 6, 371–385. https://doi.org/10.1029/91PA00384.
Ren, M., Jones, B., 2017. Spatial variations in the stoichiometry and geochemistry of Miocene dolomite from Grand Cayman: implications for the origin of island dolostone. Sediment. Geol. 348, 69–93. https://doi.org/10.1016/j.sedgeo.2016.12.001.
Saltzman, M.R., Sedlacek, A.R.C., 2013. Chemostratigraphy indicates a relatively complete Late Permian to Early Triassic sequence in the Western United States. Geology (Boulder) 41, 399–402. https://doi.org/10.1130/G33906.1.
Sano, H., 2006. Impact of long-term climate change and sea-level fluctuation on Mississippian to Permian mid-oceanic atoll sedimentation (Akiyoshi Limestone Group, Japan). Palaeogeogr. Palaeoclimatol. Palaeoecol. 236, 169–189. https://doi.org/10.1016/j.palaeo.2005.11.009.
Schlanger, S.O., Silva, I.P., 1986. Oligocene sea-level falls recorded in mid-Pacific atoll and archipelagic apron settings. Geology 14, 392–395. https://doi.org/10.1130/0091-7613(1986)142.0.CO;2.
Shackleton, N.J., 1987. Oxygen isotopes, ice volume and sea level. Quat. Sci. Rev. 6, 183–190.
Shao, L., Li, Q., Zhu, W., et al., 2017a. Neogene carbonate platform development in the NW South China Sea: litho-, bio- and chemo-stratigraphic evidence. Mar. Geol. 385, 233–243. https://doi.org/10.1016/j.margeo.2017.01.009.
Shao, L., Cui, Y., Qiao, P., et al., 2017b. Sea-level changes and carbonate platform evolution of the Xisha Islands (South China Sea) since the Early Miocene. Palaeogeogr. Palaeoclimatol. Palaeoecol. 485, 504–516. https://doi.org/10.1016/j.palaeo.2017.07.006.
Taylor, Hayes, 1980. The tectonic and geologic evolution of Southeast Asian Seas and Islands Volume 23 || The tectonic evolution of the South China Basin. Geophys. Monogr. Ser. 23, 89–104. https://doi.org/10.1029/gm023p0089.
Vahrenkamp, V.C., Swart, P.K., Ruiz, J., 1988. Constraints and interpretation of $^{87}Sr/^{86}Sr$ ratios in Cenozoic dolomites. Geophys. Res. Lett. 15, 385–388. https://doi.org/10.1029/GL015i004p00385.
Veizer, J., Buhl, D., Diener, A., et al., 1997. Strontium isotope stratigraphy: potential resolution and event correlation. Palaeogeogr. Palaeoclimatol. Palaeoecol. 65–77.
Wang, R., Yu, K., Jones, B., et al., 2018. Evolution and development of Miocene "island dolostones" on Xisha Islands, South China Sea. Mar. Geol. 406, 142–158. https://doi.org/10.1016/j.margeo.2018.09.006.
Webster, J.M., Clague, D.A., Riker-Coleman, K., et al., 2004. Drowning of the -150 m reef off Hawaii; a casualty of global meltwater pulse 1A? Geology (Boulder) 32, 249–252. https://doi.org/10.1130/G20170.1.
Webster, J.M., Clague, D.A., Faichney, I.D.E., et al., 2010. Early Pleistocene origin of reefs around Lanai, Hawaii. Earth Planet. Sci. Lett. 290, 331–339. https://doi.org/10.1016/j.epsl.2009.12.029.
Williamson, C.J., Walker, R.H., Robba, L., Yesson, C., Brodie, J., 2015. Toward resolution of species diversity and distribution in the calcified red algal genera Corallina and Ellisolandia (Corallinales, Rhodophyta). Phycologia 54 (1), 2–11. https://doi.org/10.1016/S0031-0182(97)00054-0.

Wu, S., Yang, Z., Wang, D., et al., 2014. Architecture, development and geological control of the Xisha carbonate platforms, northwestern South China Sea. Mar. Geol. 350, 71–83. https://doi.org/10.1016/j.margeo.2013.12.016.

Xu, S., Yu, K., Fan, T., et al., 2019. Coral reef carbonate $\delta^{13}C$ records from the northern South China Sea: a useful proxy for seawater $\delta^{13}C$ and the carbon cycle over the past 1.8 Ma. Glob. Planet. Change 182, 103003. https://doi.org/10.1016/j.gloplacha.2019.103003.

Yan, J.Y., Li, X.P., Zhao, L.Q., et al., 2015. Geochemistry of kaersutites in Cenozoic alkali basalts from the South China Sea: Geol. Rev, v. 61, 1434–1446 (In Chinese with English Abstract).

Yang, Z., 2014. The Evolution of Late Cenozoic Carbonate Platform in the Xisha Sea Area and Tectonic Controls. Institute of Oceanology, University of Chinese Academy of Sciences.

Yu, K., Zhao, J., 2009. Coral reefs. In: Wang, P., Li, Q. (Eds.), The South China Sea—Paleoceanography and Sedimentology. Springer, Dordrecht, pp. 229–254.

Zachos, J., Pagani, M., Sloan, L., 2001. Trends, Rhythms, and Aberrations in Global Climate 65 Ma to Present. Science 292, 686–693. https://doi.org/10.1126/science.1059412.

Zahirovic, S., Seton, M., Muller, R.D., 2014. The Cretaceous and Cenozoic tectonic evolution of Southeast Asia. Solid Earth Discuss. 5, 227–273. https://doi.org/10.5194/se-5-227-2014.

Zhang, Y., Yu, K., Qian, H., et al., 2019. The basement and volcanic activities of the Xisha Islands: evidence from the kilometre-scale drilling in the northwestern South China Sea. Geol. J. 1-13 https://doi.org/10.1002/gj.3416.